Climatic change and climatic variability: an objective decomposition

Matt Grove

Department of Archaeology, Classics and Egyptology

University of Liverpool

8-14 Abercromby Square

Liverpool L69 7WZ

United Kingdom

matt.grove@liverpool.ac.uk

Submitted: 30th June 2021

Revised: 12th September 2021

Accepted: 15th September 2021

To be published in *Quaternary Science Reviews*

Climatic change and climatic variability: an objective decomposition

Abstract

Over the past 25 years research concerning the effects of climatic fluctuations on past human societies has shifted focus considerably, with most recent hypotheses emphasizing shorter-term variability over longer-term change. Definitions of change and variability, however, remain subjective and vary considerably between researchers. It is suggested that white noise, due to its inherent unpredictability, provides a theoretically robust model of variability that accords with perceptions of variability conveyed by the existing literature. The use of white noise as a model for variability enables the development of an algorithm that objectively decomposes an empirical climatic signal into change and variability components. The algorithm, which combines singular spectrum analysis and Fourier methods, is validated via an extensive series of simulations and two empirical case studies. It is shown that the algorithm has the potential to produce genuine advances by isolating features of interest and facilitating more rigorous hypothesis testing. Its use will therefore aid researchers studying palaeoclimatic effects on prehistoric human societies as well as those studying the nature and effects of contemporary climate change.

Keywords: climatic change; climatic variability; time series; singular spectrum analysis; white noise; Southern Oscillation Index; El Niño; domestication; agriculture; Natufian.

1. Introduction

Over the past 25 years research into the possible links between palaeoclimatic change and human evolution has shifted focus considerably, with most recent hypotheses emphasizing shorter-term variability rather than longer-term change as the key challenge to ancestral human groups. This shift in focus has been driven in part by the increasing number of high-resolution palaeoclimatic and palaeoenvironmental records available, as well as by the development and application of more sophisticated methods of time-series analysis. The combination of detailed records and advanced analyses has led to a greater understanding of the complexities of prehistoric environments, with a major consequence being the development of more sophisticated, nuanced hypotheses that are more closely aligned with foundational work in evolutionary biology (Grove 2015).

The shift towards a focus on variability is particularly apparent in the fields of palaeoanthropology and Palaeolithic archaeology. Less than 25 years ago, Potts (1998a:109) was able to assert that "the most prominent narratives of hominin adaptive evolution are habitat-specific". In the intervening period, such narratives have been replaced to a great extent by hypotheses that focus on habitat generality, climatic variability, and environmental heterogeneity (e.g., Potts 1996a, 1998b; Kingston 2007; Maslin and Trauth 2009; Grove 2011a, 2011b). The idea that major developments in human evolution such as the origins of bipedalism, tool use, and widespread hunting behaviours were driven by the gradual contraction of forest cover and the concomitant expansion of savannah environments (Dart, 1925, 1953; Robinson, 1954; Washburn, 1960) has thus been substantially replaced by hypotheses such as variability selection (Potts 1996a, 1996b, 1998b), the shifting heterogeneity model (Kingston 2007; Kingston and Harrison 2007; Kingston et al. 2007) and the pulsed climate variability hypothesis (Maslin

and Trauth 2009; Trauth et al. 2010, 2014). These latter hypotheses focus on increases in behavioural flexibility, versatility, or plasticity in general, though such capacities are sometimes considered to underlie particular developments in the archaeological or fossil records (e.g., Potts and Faith 2015; Potts et al. 2018).

The exemplar of this new generation of 'heterogeneity hypotheses' is Potts' (1996a, 1996b, 1998) variability selection hypothesis (henceforth VSH). As with most subsequent heterogeneity hypotheses, the VSH takes as its starting point that fact that analyses of palaeoenvironmental proxies from various sources document a record of increasing variability over at least the past 5 Ma. Potts therefore argues that hominin evolution has been driven more by the need to adapt to this increasing variability than to any longer-term trend visible in the data, and that adaptive versatility is therefore the key to survival. This fundamental conclusion – that temporal heterogeneity promotes adaptive versatility – accords with foundational work in genetics (e.g., Levene 1953; Dempster 1955; Haldane and Jayakar 1962; Cohen 1966; Levins 1968; Lewontin and Cohen 1969; Gillespie 1973; Moran 1992; see Grove 2015), and with research examining evolutionary dynamics in fluctuating environments at broader, macroevolutionary scales (Simons, 2002; Lee and Doughty, 2003).

The progress prompted by theoretical and empirical analyses of heterogeneity hypotheses has been considerable, yet both 'variability' and 'change' remain subjectively defined. Uses of the term 'variability' are themselves highly variable, resting on an intuitive but subjective underlying notion of the "I know it when I see it" variety. The issue is complicated by the fact that variability can be identified at numerous scales, with examples in the literature ranging from fluctuations caused by the cycling of orbital eccentricity through precessional or semi-precessional timescales down to variations at the scale of human generations (e.g., Potts and Faith 2015; Potts et al. 2020; Maslin and Trauth 2009; Maslin et al. 2014; Richerson et al. 2001; Grove 2011a).

The difficulties involved in identifying the boundary between change and variability are immediately apparent in the definitions adopted by the United Nations Framework Convention on Climate Change (UNFCCC) and the Intergovernmental Panel on Climate Change (IPCC). The UNFCCC adopts the bizarre position that 'climate change' is necessarily anthropogenic whereas 'variability' is necessarily 'natural'; as noted by Pielke (2004), this position is politically rather than scientifically motivated and is of little ultimate value. The IPCC sensibly and deliberately departs from this position, providing an attempt at scientific definition. The IPCC currently defines climate change as "a change in the state of the climate that can be identified… by changes in the mean and/or the variability of its properties that persists for an extended period, *typically decades or longer*" (IPCC 2018:544, emphasis added). Climate variability, by contrast, "refers to variations in the mean state and other statistics… of the climate on all spatial and temporal scales beyond that of individual weather events" (IPCC 2018:546). The IPCC should be applauded for recognising that variability can occur on all spatial and temporal scales, but suggesting that variability 'refers to variation' merely introduces a synonym that itself remains undefined. The definition of climate change is ultimately reliant on the idea of a characteristic timescale; this is perfectly reasonable in spirit, but the typical vagaries remain. The idea that changes must persist for 'decades or longer' suggests that there is no upper bound on this timescale, and the lower bound (which is only 'typical', not universal) is quickly dissolved by counterexamples.

The El Niño – Southern Oscillation (ENSO) cycle, for example, occurs at timescales of less than a decade, but to describe one of the Earth's most important and far-reaching climate oscillations as consisting merely of 'variability' would be at odds with most scientific analyses (e.g. Aceituno 1992; Allan et al. 1996; Glantz 1996; Trenberth 1997; Larkin and Harrison 2005). Seasonal cycles occur annually by definition, but few researchers would be content to describe them simply as 'annual variability'. It is illogical to describe seasonal cycles as variability not because of the timescale at which

they occur but because they are *periodic*; the causes of this periodicity are well understood, with the result that seasonal cycles are to a certain extent predictable. A more useful operational definition would therefore identify all periodic and low-frequency components of the signal as 'change' and treat the remainder as 'variability'. The inclusion of low-frequency components as part of the 'change' retains the IPCC's intuitive notion that we must recognise change by its persistence, whilst the inclusion of periodic components prevents us from mistakenly subsuming regular patterning (even if it occurs at high frequency) within 'variability'.

At the heart of most definitions of variability – whether explicit or implicit – is the related notion of variance, or some similar (possibly non-parametric) measure of dispersion. In one of the more cogent discussions of the issue Burroughs (2005:20), for example, describes variability as "fluctuation about the mean". The variance, however, is a summary statistic; via a single scalar parameter it describes the mean squared deviation from the central tendency over an entire series of data. While this may be useful in certain circumstances, ideally the variability should be an entire time series in itself, of length equal to the original time series. A reasonable starting point for a definition of variability might therefore be the full series of deviations from some measure of central tendency, but this starting point only serves to highlight the fundamental problem: in any non-stationary time series the central tendency itself will change through time, and such change must be quantified prior to calculation of the variability. Just as the calculation of the variance depends on the prior calculation of the mean, so the calculation of the variability depends on the prior calculation of the change.

Figure 1 shows six simulated times series and is inspired by the figures and accompanying discussion provided by Burroughs (2005:19-22). The time series depicted in Figure 1a is strictly stationary and consists purely of a series of Gaussian random variates. As this series has a long-term slope of zero, most researchers would conclude that in this case the climate is variable but does not change. The time series of Figure 1b is equally simple; the change component is strictly periodic, consisting of a single sine wave, and variability is constant throughout. If variability increases, however, as it does during the course of the time series depicted in Figure 1c, it can become increasingly difficult to discern the underlying change, and therefore to separate it from the variability. This difficulty is exacerbated considerably when the change becomes even slightly more complex, as with the three superposed sine waves of Figure 1d. Further difficulties arise when either the sampling resolution or the total duration sampled are reduced (as shown in Figures 1e and 1f respectively).

~Figure 1 here~

It rapidly becomes clear that in all but the simplest cases – none of which are representative of empirical climate records – the decomposition of a time series into change and variability components is a complex problem, requiring a quantitative method that 1) reflects the intuitive notion of variability being the dispersion around some central tendency and 2) accommodates the fact that the central tendency itself is likely to be non-stationary. Three broad and overlapping categories of methods that satisfy the above conditions are available, but each depends on the subjective choice of multiple parameter values. Basic smoothing techniques involve convolution of the time series by a series of coefficients or weights; these coefficients represent a smoothing kernel such as rectangular (uniform), triangular, or Gaussian distribution. In such cases the analyst must choose the form of the kernel, the span of the kernel (i.e. the number of coefficients), and additional details of the coefficients such as the variance or bandwidth of the chosen distribution. The simplest smoothing kernel, the uniform distribution, only requires the analyst to choose the span; minimising the number of parameter choices in this way reduces subjectivity, but this form of smoothing produces undesirable effects such as the eradication or reversal of fluctuations at certain frequencies (Trauth 2015:231-5).

As the application of basic smoothing corresponds to the use of a simple lowpass filter, an alternative is to directly employ a lowpass filter with a specific frequency cut-off. However, commonly used filters in geosciences such as the Butterworth filter require specification of both the frequency cut-off (broadly comparable to the span of a smoothing kernel) and the order of the filter; more complex filters such as the Chebyshev family of filters require the specification of a greater number of parameters. Finally, various least squares methods exist that could be used for separating change and variability such as global nonlinear or polynomial least squares, local polynomials (e.g., Savitsky-Golay or spline methods), or local regression (e.g. LoESS or LoWeSS). Global methods require the specification of a polynomial order, whilst local methods require (minimally) the specification of a span as well as a choice of linear or quadratic regression.

The brief review above demonstrates that all existing methods rely on subjective parameter choices for decomposing a time series into change and variability components. All methods detailed above are theoretically valid, but their quantitative character can disguise the essentially subjective nature of their use. This subjectivity is not merely a theoretical problem; it can lead to genuine analytical inconsistencies when analysing empirical climate data. Figure 2a shows a simulated time series together with two Gaussian smoothings using different spans; when these smoothings are interpreted as the change component of the signal and the variability is calculated as the difference between the smoothed signal and the raw data, it leads to the estimates of variability shown in Figures 2b and 2c. Figure 2d demonstrates that the discrepancies between these two estimates of the variability are considerable; these two arbitrary but equally valid choices of the span of the Gaussian kernel lead to quite different assessments of the variability. It is not inconceivable that choosing different parameter values when using any of the above methods could lead to support for or rejection of the same hypothesis using the same data.

~Figure 2 here~

Although the above focuses on hypotheses rooted in palaeoanthropology and Palaeolithic archaeology, there are many instances beyond these fields in which being able to separate the 'variability' component from the 'change' component of a climatic time series allows for the resolution of fundamental questions. The algorithm outlined below, therefore, is not limited to palaeoclimatic studies, or to research in evolutionary anthropology, but has general applications in the study of historical, contemporary, and future climates. The remainder of the paper is organised as follows: Section 2 establishes white noise as a theoretically robust and mathematically tractable model for 'variability', demonstrating its essential unpredictability; Section 3 describes an algorithm for the objective decomposition of a time series into 'change' and 'variability' components. Section 4 presents a series of four simulations that validate the algorithm by demonstrating reliable, consistent performance under a wide range of different circumstances. Sections 5 and 6 act as case studies presenting empirical uses of the algorithm, the former examining the Southern Oscillation Index and the latter testing a prominent hypothesis for the origins of agriculture in southwest Asia. Finally, Section 7 briefly recapitulates and summarises the foregoing sections, discusses possible limitations of the algorithm, and considers future applications.

2. Climatic variability as white noise

A time series can be considered white noise if it consists of a series of independent, identically distributed (IID) random variables with zero mean, finite variance, and equal power across the frequency range. Importantly for what follows, this implies that the time series shows no significant

autocorrelation: the value of the time series at time t provides no information about the value of the time series at time $t + 1$. As Keshner (1982:215) memorably put it, "white noise has no memory of the past". By contrast, time series describing long-term trends, whether directional or periodic (or both) show significant autocorrelation: previous states contain significant information about the probable occurrences of future states. For an autocorrelated series the current value provides a reasonably good guess of the next value; for a white noise series, the only sensible guess is the mean of the whole series. The latter will not be a particularly good guess, but it will, on average, be the best guess. Garland and colleagues (2014) evaluate time series on an equivalent scale of *complexity*; essentially, lower autocorrelation equates to higher complexity. Accordingly, these authors state that low-complexity time series exhibit perfect predictive structure; a sine wave would be one simple example. At the other end of the scale are 'fully complex' time series such as white noise, for which "knowledge of the past gives no insight into the future, regardless of what model one chooses to use" (Garland et al. 2014:1).

Gaussian random variables are often used to simulate white noise, but white noise need not be Gaussian; series created by flipping a coin (implying a binomial distribution) or rolling a dice (implying a uniform distribution) are also white noise due to the independence criterion (flipping heads ten times in a row does not make it any more or less likely that the next flip will yield tails; rolling a six does not make it any more or less likely that you will roll another). The independence criterion is the critical point that unites the widely held (if vague) notion of 'variability' with the clearly defined, explicit mathematical definition of white noise.

In terms of the challenges posed to hominin groups, variability is often described as being unexpected, unpredictable, or uncertain (e.g. Potts 1998, 2012; Kingston 2007). Potts (1998a:85), for example, refers to the "unpredictable adaptive settings" experienced by our ancestors, and stresses how "the adaptability of human ancestors expanded over time and enhanced their capacity to respond to unexpected change and resource uncertainty" (Potts 2012:162). The lack of autocorrelation characteristic of a white noise series corresponds directly to the unpredictability noted as the key feature of variability by Potts and others. This inverse relationship between autocorrelation and predictability has been observed and exploited in several disciplines. Since Fama's foundational work on efficient markets (1970; see also Fama 1991, Lim and Brooks 2011), for example, economists have used low values of autocorrelation statistics applied to stock returns as evidence of a lack of predictability. Research in quantitative genetics has also explicitly equated low autocorrelation with unpredictability (e.g., Lande and Shannon 1996; Ashander et al. 2016; Chevin et al. 2017); in this context, it has been demonstrated that lower autocorrelation reduces the ability of a population to adaptively track environmental optima via genetic evolution (Lande and Shannon 1996).

The unpredictability of white noise relative to other signals can be quantitatively demonstrated via the application of the approximate entropy (ApEn) metric derived by Pincus (1991). ApEn is variously considered to measure sequential irregularity, complexity, instability, or simply *randomness* (e.g. Pincus 1995, 2008; Pincus and Kalman 2004; Pincus and Singer 1998; Delgado-Bonal 2019, 2020; Delgado-Bonal and Marshak 2019); all of these terms mirror the unpredictability generally considered to characterise variability in climatic time series. As predictability declines, values of the ApEn statistic described by Pincus (1991) will increase.

To demonstrate that white noise has maximal ApEn, we compare white noise signals to a series of alternative 'colours' of noise. White noise is so named because it has equal power across the frequency spectrum and is therefore broadly equivalent to the wave frequency spectrum of white light. Equivalently, blue noise contains proportionately higher spectral power at higher frequencies, whereas red noise contains proportionately higher spectral power at lower frequencies. The power

spectra of these different colours of noise can all be described by equations of the form $p = 1/f^{\alpha}$, with p equal to power, f to frequency, and α an exponent describing the colour of the noise. A noise is reddened if $\alpha > 0$, blue if $\alpha < 0$, and white if $\alpha = 0$. Noise colour is now recognised as an important characteristic of geophysical, ecological, and financial time series, and is increasingly used as a tool in modelling environmental fluctuations (e.g., Halley 1996; Halley and Kunin 1999; Halley and Inchausti 2004; Inchausti and Halley 2001; Grove et al. 2020).

Figure 3 shows median and 95 percentile ranges of lag-1 ApEn for coloured noise time series with values from $\alpha = -2$ to $\alpha = 2$, in increments of $\alpha = 0.1$. Distributions of ApEn for a given α value were calculated from 1,000 time series each of 512 time steps, generated using the Inverse Fast Fourier Transform (IFFT) method (see Press 1978; Saupe 1988; Voss 1988; Hastings and Sugihara 1993; Kasdin 1995; Grove et al. 2020; further details in Section 4). All time series were z-transformed prior to analysis, with ApEn calculations made using the default similarity criterion of 0.2 (see Chon et al. 2009; Fadlallah et al. 2013). As ApEn is a logarithmic measure (Pincus 1991), all results were exponentiated prior to graphical display. Results demonstrate that white noise ($\alpha = 0$, indicated by the dashed vertical line) is associated with maximal ApEn values, and is therefore the most complex or least predictable signal analysed. By way of a reference point, single sine waves yield exp(ApEn) values of ≈1.2, lower even than that for red noise.

~Figure 3 here~

Overall, most climatic time series have α values in the pink to red range (i.e. $1 \leq \alpha \leq 2$), meaning that they are less predictable than simple sine waves but substantially more predictable than white noise (Ditlevsen et al. 1996; Pelletier 1997; Cuddington and Yodzis 1999; Grove et al. 2020). In practice, however, palaeoclimatic time series of any appreciable length are combinations of periodic components (e.g., orbital forcing), directional trends (e.g., Miocene drying) and high-frequency variability, consistent with white noise. Only the white noise component is genuinely unpredictable, and it is therefore desirable to be able to separate this component from the remainder of the signal. The algorithm detailed below provides an objective means of achieving this separation, and therefore of isolating the unpredictable 'variability' component of the signal from the background of longer-term 'change'.

3. The Change / Variability Decomposition (CVD) Algorithm

The algorithm for decomposing a time series into change and variability components relies on Singular Spectrum Analysis (SSA; Allen and Roberton 1996; Allen and Smith 1996; Broomhead and King 1986; Ghil et al. 2002; Golyandina et al. 2001; Golyandina and Zhigliavsky 2013; Vautard and Ghil 1989; Vautard et al. 1992) coupled with a frequency domain test for white noise based on the Discrete Fourier Transform (DFT) and the theoretical expectation for the power spectrum of a white noise series. The input to the analysis is an evenly sampled time series d_n of N points and an equivalent time axis t_n. As SSA requires a (weakly) stationary time series (Vautard and Ghil 1989, Vautard et al. 1992), the input series is first de-trended by subtracting the values of a linear regression of d on t at each time step,

$$d_n \rightarrow d_n - (\alpha + \beta t_n) \quad [1]$$

Where α and β are the constant and slope of the regression equation respectively. The data are then z-score transformed (i.e. $d \rightarrow \frac{d-\mu_d}{\sigma_d}$) such that the input to the SSA is a time series with zero mean and unit variance. The coefficients of the regression of d on t (α and β) and the mean and standard

deviation of the time series prior to the z-score transformation (μ_d and σ_d) are retained so that the change and variability components of the time series can be accurately reconstructed.

A trajectory matrix $\boldsymbol{X}$ is formed of M successively lagged copies of the original time series $d_1, \ldots, d_N$, as

$$\boldsymbol{X} = \begin{bmatrix} d_1 & d_2 & \ldots & d_M \\ d_2 & d_3 & \ldots & d_{M+1} \\ \vdots & \vdots & \ddots & \vdots \\ d_K & d_{K+1} & \ldots & d_N \end{bmatrix} \quad [2]$$

Where M is the embedding dimension and $K = N - M + 1$. M is normally chosen so as to represent a lag time at least as long as the period of the longest oscillation present in the data; this can be estimated via inspection of the Fourier spectrum of the data, though the simulations of Section 4 demonstrate that the choice of M has limited effect on the output of the CVD algorithm. The lag-covariance of the time series is then calculated as

$$\boldsymbol{C} = K^{-1}\boldsymbol{X}^T\boldsymbol{X} \quad [3]$$

Where the superscript T indicates transposition. Diagonalization of $\boldsymbol{C}$ yields the $M \times M$ diagonal eigenvalue matrix $\boldsymbol{\Lambda}$ and the eigenvector matrix $\boldsymbol{P}$. The diagonal elements of $\boldsymbol{\Lambda}$ are extracted and arranged in descending order, with the eigenvectors (columns of $\boldsymbol{P}$; also referred to in SSA as the 'empirical orthogonal functions') arranged in equivalent order. The principal component matrix is given by $\boldsymbol{Y} = \boldsymbol{CP}$. Note that the eigenvectors have length M and the principal components have length K.

To convert the principal components into reconstructed components R of length N each column of the principal component matrix is multiplied by the equivalent transposed eigenvector; for R_1, for example, we calculate $\boldsymbol{Y}_1\boldsymbol{P}_1^T$, yielding a matrix of size K by M (here the subscript 1 indicates the first column). The value of R_1 at $t = 1$ is then produced by averaging along the first anti-diagonal of this matrix, the value at $t = 2$ by averaging along the second anti-diagonal, and so on. Note that whilst the values of the reconstructed components for $M \leq t \leq K$ are produced from averages of diagonals of length M, those for $t < M$ and $t > K$ are produced from averages of diagonals of lesser length; the values for $t = 1$ and $t = N$ are in fact produced by 'averaging' over single values (the values in cells $(1,1)$ and (K, M) of the $\boldsymbol{Y}_1\boldsymbol{P}_1^T$ matrix respectively). The anti-diagonal averaging procedure is then repeated for R_2 via the $\boldsymbol{Y}_2\boldsymbol{P}_2^T$ matrix and so on, concluding with the $\boldsymbol{Y}_M\boldsymbol{P}_M^T$ matrix for R_M.

$\sum_1^M R$ reproduces the original time series; the goal of the present analysis is to find an integer ω^* such that $\sum_{\omega^*}^M R$ does not differ significantly from a white noise signal. The test for conformity to white noise is performed in the frequency domain by defining successive subsets S_ω, $\{S_\omega \subseteq R | \omega \leq R \leq M\}$, $\omega = 1, \ldots, M$, summing each of these subsets, and performing a Discrete Fourier Transform (DFT) on each resultant series. The absolute magnitude of the DFT at each frequency is squared and normalized by N and the sampling frequency f_S. As one half of the symmetrical DFT output is then dropped, the remaining half is doubled, with the exception of the first frequency ($f = 0$; Trauth 2015:157ff.). The DFT output is thus transformed into a standard empirical periodogram format.

As the signal has been z-transformed prior to SSA, the theoretical spectrum corresponding to this empirical output at each frequency f is given by (Gilman et al. 1963; Priestley 1981; Mudelsee 2014)

$$\gamma(f) = \frac{2d(1-a^2)}{1-2a\cos(2\pi f d)+a^2} \quad [4]$$

For $0 \leq f \leq 1/(2d)$, where d is the sampling period (thus $1/d$ is the sampling frequency f_S and $1/(2d)$ is the Nyquist frequency) and a is the estimated autocorrelation of the series. Since for white noise $a = 0$, equation [1] reduces to

$$\gamma = 2d \quad [5]$$

at all frequencies. If we further normalize the empirical spectrum obtained via the DFT by dividing by $2d$ we have a theoretical expectation for white noise of $\gamma = 1$ regardless of the sampling frequency (for a similar approach see Torrence and Compo 1998). As the real and imaginary components of the DFT are both normally distributed and the periodogram represents the sum of the squares of these components, the empirical spectrum is distributed around the theoretical spectrum following a chi-squared distribution with two degrees of freedom, χ_2^2 (Jenkins & Watts 1968; Priestley 1981; Chatfield 1989; Bloomfield 2000; Vaughan 2005). The 95% confidence bound for the spectrum is thus $\gamma_{95} = \chi_2^2/2 = 2.9957$. If the DFT of the empirical time series is less than $\chi_2^2/2$ for $0 \leq f \leq 1/(2d)$ we can conclude that the series is not significantly different from white noise. As noted by Vaughan (2005:392) the above constitutes an exact test for a white noise spectrum, and is not subject to the problems that occur when testing models with $a > 0$.

Beginning with $\omega = 1$, successive subsets S_ω are subjected to this test; the first for which the empirical spectrum is $< \chi_2^2/2$ for $0 \leq f \leq 1/(2d)$ is denoted S_{ω^*}. $\sum_1^{\omega^*-1} R$ then constitutes the 'change' element of the SSA output and $\sum_{\omega^*}^{M} R$ constitutes the 'variability' component of that output. To translate these two separate components back into their original form, maintaining the original trend, mean, and variance of the data, the change component is computed as

$$C_d = L + \mu_d + \sigma_d \sum_1^{\omega^*-1} R \quad [6]$$

Where L is a vector of length N with $L_n = \alpha + \beta t_n$ (i.e. it returns the trend initially removed via the regression of equation [1]). The variability component is computed as

$$V_d = \sigma_d \sum_{\omega^*}^{M} R \quad [7]$$

A Matlab function for performing the above test and returning the change and variability components is available as Supplementary File 1.

4. Validation with simulated data

Any novel quantitative method should be validated with simulated data prior to empirical applications; only once the method has been shown to reliably extract the known features of simulated datasets can we be sure that the results of empirical applications will be reliable. The simulation experiments reported below were therefore designed to test whether the CVD algorithm can extract a white noise (variability) component from time series that contain other components frequently found in (palaeo)climatic signals. The signal in Simulation 1 consists of a mixture of periodic components and white noise (with the amplitude of the white noise component exhibiting marked changes), whilst the signal in Simulation 2 consists of a mixture of periodic components, red noise, and white noise. Indicative examples are explored for both simulated signals; for the second simulated signal, which represents the more demanding test of the algorithm, a full range of simulations are assessed over a range of relative variances of the periodic and red noise components in Simulation 3. Finally, Simulation 4 examines the effects of variation in M - the one free parameter in the CVD algorithm – on the resulting estimates of the change and variability elements.

4.1. Simulation 1

The simulated signal consists of 500 time steps of two superposed sine waves with periods of 23 and 59 time steps. To this signal is added a contant of 10, a linear trend of -0.02 units per time step and Gaussian white noise with a standard deviation equal to:

- 0.5 in time steps 1 to 200 and 301 to 500;
- 2 in time steps 201 to 300.

Formally, the value of the signal d at time t is given by

$$d(t) = -0.02t + 10 + \sin(2\pi t/23) + \sin(2\pi t/59) + \varepsilon \quad [8]$$

Where

$$\varepsilon = \begin{cases} \mathrm{N}(0,2) \text{ if } 200 < t < 301 \\ \mathrm{N}(0,0.5) \text{ otherwise} \end{cases} \quad [9]$$

For the purposes of the analysis, the 'variability' element of the signal is defined as the Gaussian white noise component; the 'change' element of the signal is the therefore the combination of the two sine waves and the linear trend. As the periods of the sine waves are known, the embedding dimension for the SSA is set to $M = 60$. Since ε is a random variable, each realisation of the signal d will have a slightly different form. The results below examine one such realisation; more comprehensive simulations using more complex signals are described under Section 4.3.

Figure 4 shows an example of the CVD algorithm applied to the simulated signal described above. As would be expected from the basic logic of SSA, the number of reconstructed components comprising the change element of the signal (S_{ω^*}) is equal to four in this example: one pair in quadrature representing the 23-unit period sine wave and another pair in quadrature representing the 59-unit period sine wave. The remaining $M - S_{\omega^*} = 56$ reconstructed components comprise the variability element of the signal. Though it is clear from Figure 4b that some of the variability element leaks into the change element during the high variability phase (time steps 201-300), Pearson product-moment coefficients describing the correlations between the original and reconstructed elements indicate that greater than 90% of the original signal is recovered for both the change and variability elements.

~Figure 4 here~

4.2. Simulation 2

The second simulated signal used to test the CVD algorithm is identical to that described in Simulation 1 except that the linear trend is replaced by a red noise element. The background signal of empirical (palaeo)climatic records is often found to be in the pink to red range (Cuddington and Yodzis 1999; Ditlevsen et al. 1996; Lovejoy and Shertzer 1986; Mandelbrot and Wallis 1969; Pelletier 1997); as such, the ability to decompose a signal consisting of periodic, red noise, and white noise elements is an important benefit of the CVD algorithm. Red noise is generated via the Inverse Fast Fourier Transform (IFFT). Assuming an arbitrary sampling frequency of unity and a timescale t of $N/2$ integer units, a frequency scale is established as $f = (t/2)/(N/2)$. Amplitudes corresponding to red noise in the frequency domain are then calculated as $A_f = \sqrt{0.5(1/f^2)}$, after which A_f is doubled in length by adding a mirrored version to the bottom of the existing vector. A vector of N random phase angles $\theta \in [0, 2\pi]$ is generated and the final vector $V = A_f e^{\sqrt{-1}\theta}$ is passed to the IFFT, with only the standardized, real component $\Re$ of the resulting complex output retained. The full value of the signal d at time t is therefore given by

$$d(t) = \Re + \sin(2\pi t/23) + \sin(2\pi t/59) + \varepsilon \quad [10]$$

Where ε is given by equation [9].

For the purposes of the analysis, the 'variability' element of the signal is defined as the Gaussian white noise component; the 'change' element of the signal is the therefore the combination of the two sine waves and the red noise. As above, the embedding dimension for the SSA is set to $M = 60$. As per Simulation 1, the fact that $\Re$ and ε are random variables implies that each realisation of the signal d will be different; this variation is examined in more detail under Section 4.3.

Figure 5 shows an example of the CVD algorithm applied to the simulated signal described above. In this example $S_{\omega^*} = 5$; four components represent the two sine waves, with the red noise represented by a single component. Given the length of the series relative to the embedding dimension ($N = 500$, $M = 60$) and the fact red noise is by definition dominated by the relatively high amplitude of relatively low frequencies, it is not surprising that in this example the red noise element is represented by a single reconstructed component. The red noise element simulated here is stochastic, however, and S_{ω^*} will vary considerably in line with this stochasticity (see Simulation 3, below). SSA will automatically group oscillations at frequencies $< 1/M$ as trend components; although there is no definitive, automated method for choosing M for an empirical time series, this suggests that larger values of N/M will lead to smaller values of S_{ω^*}. As per Simulation 1, some of the variability element leaks into the change element during the high variability phase; however, again the Pearson product-moment coefficients describing the correlations between the original and reconstructed elements indicate that greater than 90% of the original signal is recovered for both the change and variability elements.

~Figure 5 here~

4.3. Simulation 3

Simulation 3 uses essentially the same time series as Simulation 2, but allows the sine wave, red noise, and white noise components to vary in relative amplitude across simulations. Three sets of simulations were performed: in each, one of the three components takes on variances between 0.25 and 4 in 16 logarithmically equal increments while the other two components are stabilised with variances of unity. This allows for analysis of the effects of changes in the variance of each component separately; furthermore, because in each simulation two components were processed to have unit variance, changes in the variance of the third component can be read as direct multiples of the variances of the other components (e.g., when white noise has a variance of 2, this means that its variance is twice that of both the sine wave and red noise components). In each simulation 1,000 time series were generated at each increment; Pearson product-moment correlations between the known (generated) change and variability and the change and variability recovered by the CVD algorithm were calculated for each time series, with overall results presented as the median correlation plus or minus the median absolute deviation in correlation. Note that each individual time series analysed differs due to stochastic generation of the white and red noise components; the underlying sine wave component is identical in form in each time series.

The results of these simulations are shown in Figure 6. Figure 6 panels a-c indicate that recovery of the change component diminishes as white noise variance increases, improves as sine wave variance increases, and is relatively unaffected by changes in red noise variance. Figure 6 panels d-f indicate that recovery of the variability component diminishes as red noise variance increases, is relatively unaffected by sine wave variance, and rapidly improves as white noise variance increases up to the point at which its variance is roughly equal to that of the summed red noise and sine wave variances,

after which it slowly declines. Importantly, these simulations reveal that the median correlation never falls below 0.8, suggesting that a substantial proportion of both the change and variability components is recovered under all conditions analysed.

~Figure 6 here~

4.4. Simulation 4

A major criticism levelled at the use of existing methods for the assessment of change and variability above is that they rely on numerous subjective parameter choices. The CVD algorithm, however, does contain a single free parameter – the embedding dimension (M). The simulations reported below document the effects of variation in M on the resulting estimates of the change and variability components. In standard SSA the choice of M is based on a trade-off between the need to capture sufficient information about low-frequency components (favouring large M) and the need for sufficient repetitions of the embedding window over the total length of the time series (favouring small M/N). Vautard and colleagues (1992:102) suggest that SSA is successful at identifying periodicities in the range $M/5$ to M, and further that one should chose M small enough to allow at least three repeats of the window (i.e., $M \leq N/3$). The CVD algorithm, however, is not concerned with identifying significant periodicities in the data – existing Monte Carlo SSA methods are sufficient to achieve this (Allen and Robertson 1996; Allen and Smith 1996; Groth and Ghil 2015). As demonstrated below, the CVD algorithm is therefore far less dependent on the choice of M than is standard SSA.

The experiments below were carried out using pink noise as the signal subject to decomposition. Pink noise is a good approximation for many climatic data sets (Ditlevsen et al. 1996; Pelletier 1997; Cuddington and Yodzis 1999), and the fact that its power varies directly as the reciprocal of frequency makes it a particularly hard signal to decompose. The results are therefore conservative regarding the magnitude of the effect of varying M. 100 pink noise time series of $N = 300$ time steps were generated using the IFFT method (see above); each was then subject to the CVD algorithm using 19 different values of M ranging from 10 to 100 in increments of 5. The resulting change and variability output were saved as separate $N \times 19$ matrices, and their variance-covariance matrices calculated. These variance-covariance matrices were then averaged over all 100 signals to estimate the differences in estimates of change and variability caused by variation in M. ω^* was also recorded for each of the 100*19 analyses to examine how it changes in response to changes in M.

Figure 7a shows that ω^* increases approximately logarithmically with M, although there is considerable variance around this broad trend. That ω^* covaries positively with M is important, however, because this relationship stabilises the resulting estimates of change and variability. As M increases, the number of eigenvectors (or reconstructed components) used to characterise *both* the change *and* the variability elements increases, leaving the relationship between these two elements relatively stable. Figure 7b shows that, over an order of magnitude difference in M, estimates of variability and change remain remarkably consistent; the smallest correlation coefficients between estimates are >0.93, and most of the differences occur at either end of the series where the effects of different embedding dimensions are greatest (see Figure 8 for an individual example).

~Figure 7 here~

~Figure 8 here~

There is therefore far greater latitude in choosing M when using the CVD algorithm than when employing MC-SSA to identify significant periodicities in a time series. This is partly due to the fact that all periodic components with periods $> M$ will be subsumed into the change component of the

SSA output (Vautard and Ghil 1989; Ghil et al. 2002) and partly due to the documented positive covariation between ω^* and M. Although M is a 'subjective parameter' in the CVD algorithm, therefore, it has little effect on the resulting assessment of the change and variability components / elements. In some analyses there will be a clear *a priori* empirical rationale for the choice of M (see Section 5 for an example); in analyses where this is not the case, the above results provide confidence that the choice of M will have minimal bearing on the estimation of change and variability. Where the choice of M is totally 'naïve' (i.e. there is no underlying expectation, and no significant periodicity evident in preliminary spectral analyses) simulations like those above could be used to verify the effects of varying M, but in most analyses this is unlikely to be necessary.

5. Case Study: The El Niño – Southern Oscillation

The first case study examines a time series describing the atmospheric component of the El Niño – Southern Oscillation, a fundamentally important climatic cycle that has often been subject to SSA-based analyses, has wide-ranging global impacts, and is also recognised as having had substantive effects on prehistoric climates (e.g. Kaboth-Bahr et al. 2021). El Niño events weaken or even reverse the normal easterly trade winds in the equatorial Pacific Ocean, increasing the depth and decreasing the slope of the ocean thermocline and preventing upwelling of nutrient-rich water in the east. Warmer waters in the eastern equatorial Pacific decrease atmospheric pressure, disrupting the Walker Circulation and causing a southward shift of the Pacific jet stream. Proximate effects include increased precipitation in coastal South America and drought in Indonesia and Australia; however, El Niño's strong teleconnections can ultimately lead to increased storm frequency in the coastal states of North America, weaker monsoons in Southeast Asia and even more pronounced rainy seasons in sub-Saharan Africa (Nicholson and Selato 2000). Whilst El Niño events cause floods in South America and droughts in Australasia, the inverse of this pattern is found when the trade winds are strengthened during La Niña events. Technically El Niño and La Niña events represent the opposite poles of an oceanic phenomenon, but this cannot be meaningfully decoupled from the associated atmospheric phenomenon referred to as the Southern Oscillation. The term ENSO (El Niño – Southern Oscillation) thus encompasses the full oceanic-atmospheric cycle, a cycle closely linked to the Walker Circulation and thus to climatological patterns across the planet (Allan et al. 1996; Power et al. 1999; Vecchi et al. 2006).

The climatic anomalies caused by El Niño events have pervasive ecological consequences. Reduced upwelling in the eastern equatorial Pacific leads to a nutrient deficit and reduced phytoplankton populations, with cascading effects at higher trophic levels including reduced fish populations along the eastern Pacific coast from Chile to Alaska (Barber and Chavez 1983; Bakun and Broad 2003). Terrestrial effects are equally pervasive, with far-reaching effects on floral, avian, and mammalian species. In the eastern Pacific, plant cover on the normally barren islands of the Gulf of California can increase from 0-4% to 54-89% during El Niño years (Polis et al. 1997), while in Australia and Northern Sumatra drought conditions inhibit the ability of mangroves to produce a defensive toxic sap, leaving them susceptible to defoliation by lepidopteran larvae (McKillup and McKillup 1997). On a broader scale, Tian and colleagues (1998) suggest that the hot, dry weather experienced in the Amazon Basin forest during El Niño years converts the area from a carbon sink to a source of atmospheric carbon (see also Humphrey et al. 2018). The wider ENSO phenomenon is now recognised as the most important single driver of the terrestrial carbon cycle (Cox et al. 2013; Betts et al. 2016). Droughts caused by El Niño events can lead to widespread forest fires with long-lasting effects on ecological dynamics, particularly in tropical Asia (Liu et al. 2017). Chen and colleagues (2017) calculate that, for

the 1997-2016 period, fire emissions from tropical forests in El Niño years were 1.33 times greater than those in La Niña years.

Increases in primary productivity due to wetter conditions also have terrestrial effects at higher trophic levels; initial population increases in herbivores are followed by subsequent increases in carnivore numbers (Jaksic et al. 1997; Wright et al. 1999; Grant et al. 2000). Jaksic (2001) demonstrates that populations of small rodents in western South America increase dramatically within months of increased El Niño rains; increases in larger rodent populations show a greater lag and are less pronounced. Increases in predator numbers occur approximately a year after increases in their prey, with effects again more pronounced in smaller-bodied animals. Letnic and colleagues (2005) find similar patterns in central Australia during La Niña periods, also noting an increase in avian predators of small rodents such as black-shouldered kites (*Elanus axillaris*). Studies of individual avian species on oceanic islands have revealed equally profound patterns; on the Galapagos island of Daphne Major, for example, two species of Darwin's Finches (*Geospiza fortis* and *G. scandens*) showed extended breeding seasons, greater brood production, and increased clutch sizes during El Niño years (Grant et al. 2000).

ENSO fluctuations are monitored via numerous continuous sea surface temperature (SST) and atmospheric pressure measures, yet there remains no universally agreed definition of what constitutes an El Niño (or La Niña) event (e.g. Aceituno 1992; Glantz 1996; Trenberth 1997; Larkin and Harrison 2005). In terms of SST, there exists disagreement over which region of the equatorial Pacific is most indicative of ENSO cycling. Initial efforts focused on the Niño 3 (5°N-5°S, 90°-150°W) or, less frequently, Niño 4 (5°N-5°S, 160°E-150°W) regions; more recently the Niño 3.4 region (5°N-5°S, 170°W-120°W) has risen to prominence, as this longitudinal compromise appears to better represent average SSTs across the equatorial Pacific. SST time series are generally presented not as raw data but as excursions relative to the mean (and sometimes the standard deviation) of some base period (e.g. the base period of 1950-1979; see Trenberth 1997). As noted by Trenberth (1997), the choice of base period can of course have marked effects on the calculation of excursions. To reduce noise in the resultant time series, data are often presented as 3- or 5-monthly running means.

The foregoing vagaries notwithstanding, NOAA currently defines an El Niño event as "a positive sea surface temperature departure from normal (for the 1971–2000 base period) in the Niño 3.4 region greater than or equal in magnitude to 0.5°C, averaged over three consecutive months" (https://www.cpc.ncep.noaa.gov/products/precip/CWlink/MJO/enso.shtml). This 3-month running mean excursion relative to the 1971-2000 base period is referred to as the Oceanic Niño Index (ONI). The atmospheric component of ENSO, by contrast, has predominantly been quantified via the Southern Oscillation Index (SOI), a standardized measure of the difference in mean sea-level air pressure between Tahiti (French Polynesia; 17°21′S, 210°29′E) in the east and Darwin (Australia; 12°28′S, 130°50′E) in the west. There are many advantages to the SOI as an ENSO indicator: it is relatively simple to calculate, is tightly correlated with changes in ocean temperatures across the eastern tropical Pacific, and measurements reach further back in time than those for SSTs (for which values prior to 1950 are often reconstructed from other proxies rather than directly measured). It is also worthy of note that the Niño 3.4 SST series has achieved primacy among analysts at least partly because it correlates better with the SOI than do either the Niño 3 or Niño 4 series.

The analyses below therefore employ the monthly SOI time series from January 1870 to December 2019 (Ropelewski and Jones 1987; Allan et al. 1991; data obtained from https://crudata.uea.ac.uk/cru/data/soi/). The CVD is performed to eliminate high-frequency variability, permitting a clearer analysis of the periodic (and quasi-periodic) ENSO components that are the principal drivers of the major fluctuations, and facilitating identification of El Niño events. The

focus here is on El Niño, but one could equally use the technique to examine the dynamics of La Niña. The analysis is designed to pick out pronounced troughs in the raw SOI and in the 'change' output of the CVD, and to compare these to identified El Niño events (Smith and Sardeshmukh 2000); it is demonstrated that employing the 'change' component of the SVD makes meaningful troughs more apparent, reduces the frequency of false positive El Niño identifications, and detects a series of El Niño events more consistent with current estimates of their chronology. The focus is therefore on the central chronological locations of events rather than their duration, though in some cases it becomes clear that single events consist of multiple troughs.

As stated above, definitions of El Niño events remain contentious; nonetheless, a comparison of events identified via the raw SOI and the 'change' component of the CVD with a robust chronology remains an important aspect of any evaluation of the CVD. The chronology employed here is that developed by Smith and Sardeshmukh (2000; data obtained from https://www.psl.noaa.gov/people/cathy.smith/best/#years). Smith and Sardeshmukh (2000) standardised (i.e., z-scored) both the SOI and the Niño 3.4 SST time series over the period from 1870 to 2019, then calculated 'strong' El Niño months as those in which both times series exceeded the 20th percentile; 'weak' El Niño months were defined as those in which both time series exceeded the 33rd percentile. Both the 'strong' and 'weak' indices are employed below.

The CVD algorithm was applied to the monthly SOI series, employing M = 60 months; this embedding value corresponds to a five-year period and is frequently employed in SSA analyses of the SOI (e.g., Keppenne and Ghil 1992; Allen and Smith 1996). The ω^* value demonstrates that the first 15 reconstructed components are retained to form the 'change' element of the decomposition whilst the remaining 45 form the 'variability' element. The CVD removes a substantial part of the high-frequency variation in the SOI, as shown in the spectral analysis of Figure 9. Following application of the CVD, a simple algorithm is used to define troughs in both the raw SOI and the 'change' component that predict chronological locations of El Niño events: a trough is a value that is less than either of the adjacent values and also less than -1 (Kiladis and van Loon 1988). Use of this algorithm leads to the identification of events in the raw SOI (Figure 10a) and the 'change' element of the CVD (Figure 10b). The chronology of both 'strong' and 'weak' El Niño months (following Smith and Sardeshmukh 2000) is displayed at the base of each figure, with individual identified troughs indicated as consistent (red triangles) or inconsistent (black triangles) with this chronology. An identified trough is regarded as consistent with the chronology if it falls within either a 'weak' or a 'strong' El Niño month as identified by Smith and Sardeshmukh (2000).

~Figure 9 here~

It is immediately apparent that use of the CVD reduces the number of false positives (black triangles in Figure 10) relative to use of the raw SOI. Table 1 demonstrates that the reduction in false positives is approximately 11-12%; this constitutes an important advance, as it provides a considerably better correspondence with the chronology developed by Smith and Sardeshmukh (2000) and allows for clearer delineation of true El Niño events. Of equal importance is the reduction in the number of troughs identified per El Niño event; this reduction makes it considerably easier to identify maximal El Niño states and to examine their periodicity. Simple histograms of inter-event periods (Figure 11) demonstrate the improvement in the signal afforded by the CVD; after removing sub-annual periods from both signals it is clear that the distribution of inter-event periods for the raw SOI shows positive skewness with most values in the 1-2 year bin. The distribution of inter-event periods for the 'change' component of the CVD, however, shows a distinct mode in the 3-4 year bin, consistent with the average periodicity of El Niño events (Trenberth 1997).

~Figure 10 here~

~Figure 11 here~

~Table 1 here~

There are therefore clear empirical advantages of employing the CVD to examine the SOI time series; in addition, there are clear theoretical advantages. Monthly time series of the SOI (and other El Niño indicators) are often smoothed using either 3- or 5-month running means. However, the choice of 3 or 5 months for the smoothing is arbitrary, and the two alternatives necessarily lead to different results. Furthermore, as noted by Trauth (2015:234-5), the use of running means is undesirable as it can eliminate elements of the frequency response and can even lead to inversion of the signal. The use of Gaussian smoothing or the careful design of frequency-specific filters avoids such issues, but requires the analyst to choose a window width, parameters of the smoothing kernel, or a type of filter and an associated frequency band. The CVD, by contrast, employs a data-driven approach to remove low-variance, high-frequency components of the signal; the 'change' component therefore gives an empirically justified reconstruction of the long-term dynamics.

The above analysis demonstrates the value of employing the CVD to examine the SOI in relation to El Niño events; however, such analyses could certainly be taken further. Future analyses should consider the Niño 3.4 SST series as well as the SOI, and there would be value in applying the CVD to individual components of these composite indices; for example, application of the CVD separately to the Tahiti and Darwin sea-level air pressure time series prior to construction of the SOI could lead to greater clarity in pinpointing El Niño events. The CVD may also prove useful in generating predictions of future ENSO activity; since the CVD can be used to remove variability, the 'change' component analysed above provides a useful baseline for prediction. If 'change' and 'variability' are equated with 'signal' and 'noise' then future predictions can be based on the 'signal' component, with the distribution of the 'noise' used to produce confidence intervals encompassing known historical variability.

6. Case Study: The origins of agriculture in southwest Asia

As with many other aspects of human evolution, there is a considerable history of research into the links between climatic change and the origins of agriculture (e.g., Richerson et al. 2001; Bettinger et al. 2009; Moore and Hillman 1992; Bar-Yosef and Belfer-Cohen 1992, 2002; Bar-Yosef 1998; Henry 1989, 1995, 2013; Hillman 1996; Wright 1968, 1976, 1993; Childe 1928; Flannery 1969; Braidwood 1960; Braidwood and Braidwood 1953; Braidwood and Howe 1960). Childe (1928) suggested that agriculture was one possible strategy adopted to mitigate climatic changes at the onset of the Holocene. The prevailing climatic model of the time suggested that high-latitude glacials equated to pluvial phases at lower latitudes; as such, the onset of the Holocene interglacial was seen as a period of environmental drying, punctuated spatially by oases acting as refugial zones for plants, animals and humans. Childe identified the Near East as one such oasis, and prompted the future work by Braidwood and Wright that reversed this climatic interpretation, demonstrating the generic pattern of cold, dry glacials and warm, wet interglacials in the region (e.g. Braidwood 1960; van Zeist and Wright 1963; Wright 1968, 1976).

The revisions resulting from Wright's (1968, 1976, 1993) research, together with an increasingly comprehensive understanding of the chronology and conditions of the last glacial termination (e.g. Rasmussen et al. 2006), led to the prevalence of a second major hypothesis. Moore and Hillman (1992) argued that the cool, dry conditions of the Younger Dryas (henceforth YD) reduced the availability of

wild plant foods relative to the preceding Bølling-Allerød (henceforth BA) and that this reduction in the resource base prompted human groups to accelerate incipient experiments in crop domestication, leading to the origins of agriculture (see also Wright 1993; Bar-Yosef 1998; Bar-Yosef and Belfer-Cohen 2002; Blockley and Pinhasi 2011). Although this latter hypothesis has remained prevalent, several weaknesses in its explanatory ability have become apparent as the dating of the relevant archaeological sequences has become more detailed.

Most debates on the origins of agriculture in the Near East revolve around the Natufian, and to a lesser extent on the succeeding early aceramic phase (the Pre-Pottery Neolithic A, henceforth PPNA). In its current form, the Moore and Hillman (1992) hypothesis rests on the alignment of the Early Natufian with the BA and the Late Natufian with the YD. It also depends, to a lesser extent, on the demonstration of increasing sedentism, increasing percentages of 'founder crop' progenitors in archaeobotanical assemblages, and greater evidence of the elements of material culture associated with their processing. The first appearance of the Early Natufian closely postdates the onset of the BA, suggesting that the large settlements, semi-circular stone structures, burials, symbolic artefacts, and possible storage facilities of this period indicate an increasingly sedentary lifestyle facilitated by the BA climatic amelioration. However, recent evidence suggests that the Late Natufian began perhaps 300-600 years prior to the onset of the YD in the Mediterranean (Henry 2013; Grosman 2013; Caracuta et al. 2016), and that archaeological signatures of the Early and Late Natufian show considerable chronological overlap (Barzilai et al. 2017). This casts considerable doubt on the hypothesis that the Late Natufian was a response to the YD specifically but, as Blockley and Pinhasi (2011) note, the beginnings of the Late Natufian may still coincide with climatic deterioration evident during the Allerød oscillation (see Figure 12).

~Figure 12 here~

The prevailing archaeological picture is of increased sedentism in the Early Natufian followed by a return to smaller, more ephemeral sites and greater mobility in the Late Natufian (Goring-Morris and Belfer-Cohen 1997; Bar-Yosef and Belfer-Cohen 2002; Munro 2004), though some degree of sedentism may have persisted in the southern Levantine Mediterranean core zone (Richter et al. 2017). Ground stone artefacts increase in frequency during the Natufian, and are more numerous in later phases (Rosen and Rivera-Collazo 2012); sickles show a similar pattern (Maeda et al. 2016), but the precise meaning of their presence is clouded by similar artefacts from Upper Palaeolithic sites in the region such as Wadi Kubbaniya and Ohalo II (e.g. Snir et al. 2015; Arranz-Otaegui et al. 2018a). Finally, the archaeobotanical evidence of the last decade casts doubt upon the conception of Late Natufian peoples as incipient agriculturalists. Rosen (2010) suggests that the Natufians responded to environmental deterioration by exploiting a wider variety of plant foods, without a particular focus on cereals. Analysing the extensive archaeobotanical record from Shubayqa 1, Arranz-Otaegui and colleagues (2018a) argue that founder crop progenitors were not an integral component of Natufian subsistence and did not become so until the early Pre-Pottery Neolithic B (henceforth PPNB). Instead, evidence from this site suggests that club-rush tubers were a primary source of plant food in the Early Natufian (Richter et al. 2017; Arranz-Otaegui et al. 2018b).

A third hypothesis, evaluated below via the CVD algorithm, focuses not on the increases in temperature and precipitation created by the last glacial termination, but on the concomitant reduction in climatic variability. Richerson and colleagues (2001; see also Bettinger et al. 2009) advance the provocative hypothesis that "agriculture was impossible during the last glacial" but was ultimately "compulsory in the Holocene" (Richerson et al. 2001:388). Although these authors reference the more arid climates and lower CO_2 levels of the last glacial, the central plank of their argument is that the high-amplitude, high-frequency fluctuations of the period made the necessarily

high investments in and delayed returns of agriculture inefficient and unreliable (Bettinger et al. 2009). Rather than the YD providing a stimulus to further exploitation of founder crop progenitors, these authors argue that it simply stalled any incipient agricultural experiments undertaken among the Early Natufians during the relative amelioration of the BA (see also Feynman and Ruzmaikin 2007).

The 'variability hypothesis' of Richerson and colleagues (2001) is more nuanced than it first appears, and takes into account the contingencies of cultural innovation and transmission in the various independent 'centres of origin' in which agriculture emerged. To be clear, the Holocene decrease in climatic variability could not possibly have *caused* the evolution of agriculture, but it could certainly have *facilitated* it; the fact that agriculture did evolve in at least 11 geographically independent centres during the Holocene (Larson et al. 2014; Fuller et al. 2014) suggests that the benefits for plant cultivation of a relatively stable climate were repeatedly recognised and exploited by humans during this period. As the region in which agriculture developed the earliest, the Near East provides a particularly germane archaeological case study with which to test the variability hypothesis; evidence of agricultural development prior to a significant reduction in climatic variability would falsify the hypothesis, at least in relation to this region.

To construct a test of the variability hypothesis, the CVD algorithm was applied to the last 25 ka of the 20-year mean NGRIP oxygen isotope data using the GICC05 timescale (Grootes and Stuiver 1997; Johnsen et al. 1997; Stuiver and Grootes 2000; NGRIP Members 2004; Rasmussen et al. 2014; Seierstad et al. 2014), with M = 100 (= 2,000 years). Although NGRIP is a high-latitude record, there is comprehensive evidence that the fluctuations it displays are very similar to those seen in regional Near Eastern records (e.g. Bar-Matthews et al. 1999, 2000, 2003; Vaks et al. 2006; Robinson et al. 2006). The correlations between the NGRIP records and those from the Soreq and Peqiin Cave speleothems, as well as with eastern Mediterranean marine core records, are particularly striking (Bar-Matthews et al. 2003). Furthermore, NGRIP $\delta^{18}O$ fluctuations are closely tied to total tree taxa percentages in pollen records from southern Europe such as those from Lake Ohrid (e.g. Sadori et al. 2016; Sinopoli et al. 2018) and Tenaghi Philippon (e.g. Milner et al. 2012, 2013, 2016; Wulf et al. 2018).

Following isolation of the variability component of the NGRIP $\delta^{18}O$ signal, statistically significant increases and decreases in variability were identified using the running Mann-Whitney test proposed by Trauth and colleagues (2009; Trauth 2015) on absolute values of the first derivative of the variability component. Note that the running Mann-Whitney is preferred to the running Ansari-Bradley test in this case as the key question relates to the absolute magnitude of the variability component. Following the recommendations of Trauth and colleagues (2009) this test was performed using three separate window widths (of 50, 100, and 150 data points [=1000, 2000, and 3000 years]); transitions in the magnitude of the variability were deemed significant only if all three window widths yielded simultaneous significant results at α = 0.99.

The results of the above analysis are summarised in Figure 13. Four statistically significant transitions were observed: increases in variability at 12,990 – 13,260 BP and 9,060 BP, and decreases in variability at 14,760 – 14,980 BP and 11,810 BP. Where boundaries rather than point dates are given, this is because in some cases smaller windows suggest multiple significant results whereas larger windows clearly demonstrate that these multiple significant results were components of the same transitions (see Figure 13, bottom panel). Smaller windows therefore help to localize transitions in time, whereas larger windows ensure that protracted transitions are not interpreted as multiple separate events. In terms of the overall palaeoclimatic chronology, the decreases in variability at 14,760 – 14,980 BP and 11,810 BP correspond broadly to the onset of the Bølling-Allerød and the start of the Holocene respectively. The increase in variability at 12,990 – 13,260 BP predates the onset of the Younger Dryas

by ~90 years, and the small but significant increase at 9,060 BP occurs well within the Holocene, has not been previously recognised, and broadly coincides with the end of the PPNB.

~Figure 13 here~

The dates of these transitions in the magnitude of variability are next compared to two archaeological datasets documenting the origins of agriculture in southwest Asia. The first is a general chronology of key plant domestication dates for southwest Asia compiled by Larson and colleagues (2014). These authors document three important phases in the domestication process: 1) exploitation prior to domestication; 2) management or pre-domestication cultivation, and; 3) the appearance of the morphological changes associated with domestication. In terms of testing the variability hypothesis, only (2) and (3) can be regarded as evidence for domestication, but (1) provides a useful addition, particularly given the debate surrounding the exploitation of 'founder crop' progenitors during the Natufian period outlined above.

The alignment of this chronology with the dates of the variability transitions highlighted via use of the CVD algorithm is shown in Figure 14. It can be seen from this figure that, although pre-domestication exploitation of founder crops may have begun prior to the transition to low variability at 11,810 BP, management and cultivation occurred only after this transition. This pattern supports the variability hypothesis in terms of the Holocene decrease in variability acting as a possible precursor to domestication, but also raises the intriguing question of why there is such limited evidence for founder crop exploitation during the Early Natufian (e.g. Rosen 2010; Asouti and Fuller 2012; Arranz-Otaegui et al. 2018a), which corresponds to a period of reduced variability associated with the Bølling-Allerød. Several researchers (e.g. Rosen 2010; Asouti and Fuller 2012) have suggested that Early Natufian plant exploitation was highly diversified rather than being focussed on cereal and pulse crop progenitors, and it may simply be the case that this broad pattern of consumption prevented the need for active investment in particular plant resources. On the other hand, evidence for the production of flour from wild grasses as early as 23 ka (Piperno et al. 2004; Snir et al. 2015) and the production of breads made of wild einkorn and club-rush tubers by 14.4 ka (Arranz-Otaegui et al. 2018b) suggests that there may have been numerous "false starts and dead ends" (Fuller et al. 2012:619) on the road to the eventual widespread adoption of cultivars.

~Figure 14 here~

The second dataset was collated by Arranz-Otaegui and colleagues (2018) and consists of the percentages of founder crops among the non-woody plant macro-remains at 35 southwest Asian archaeological sites dated to between 15 and 9.7 ka cal. BP. Following Weiss and Zohary (2011), the eight founder crops are identified as einkorn, emmer, barley, lentil, pea, chickpea, bitter vetch, and flax. Arranz-Otaegui and colleagues (2018:278) perform a Pearson correlation on these data to demonstrate the increase in percentages of founder crops through time. However, it is clear from the accompanying plot (Arranz-Otaegui et al. 2018:279) that the linear fit implied by the correlation may not be the best characterisation of the trajectory demonstrated by these data. While the analysis presented by Arranz-Otaegui and colleagues (2018) is certainly valuable in demonstrating the increase in percentages of founder crops, the analyses reported here fit an alternative sigmoid model to the data.

Following Trauth and colleagues (in press), the sigmoid fit is described as

$$F = a + \frac{b}{1+e^{-c(-t+d)}} \quad [11]$$

Where F is the percentage of founder crops in the assemblage, t is the age of the assemblage in years cal. BP and a, b, c, and d are model parameters. The value of the sigmoid is that it allows for the identification of the transition date at which the greatest increase in percentages of founder crops in these assemblages takes place. The parameter d estimates the most likely date of this transition, and the 95% confidence intervals on this parameter can be used to provide a probabilistic estimate of when the most rapid increase in founder crop percentages occurred. a is the mean equilibrium percentage of founder crops prior to the transition, $a + b$ is the mean equilibrium percentage of founder crops after the transition, and c is proportional to the speed of the transition.

Figure 15 shows the sigmoid fit together with the dates of decreases and increases in variability demonstrated via CVD analysis of the NGRIP $\delta^{18}O$ data. The mean percentage of founder crops in the assemblages increases from 5.6% to 44.1%; the 95% confidence interval on the d parameter demonstrates that 95% of this increase occurs between 11,997 and 10,545 cal. BP, with a mean transition date of 11,270 cal. BP. Although the start of this transition at 11,997 cal. BP predates the decrease in variability at 11,810 demonstrated via the CVD analysis this occurs during a gap in the archaeological data of around 600 years between the assemblages from Mureybet I-II (c. 12,300 cal. BP) and Hallan Çemi (c. 11,700 cal. BP). As above, therefore, the results of this second analysis also support the variability hypothesis of Richerson and colleagues (2001). The lack of significant evidence for cultivation during the low-variability phase associated with the Bølling-Allerød proves that low variability alone is not sufficient to lead to agriculture, precluding strict environmentally determinist arguments for the origins of plant domestication (cf. Roberts et al. 2018). Cultural responses to the environmental conditions of the Holocene, however, led to the rapid development of agriculture in southwest Asia following the decrease in variability documented via the CVD algorithm.

~Figure 15 here~

7. Recapitulation and Conclusions

As stated in Section 1, hypotheses concerning the effects of climatic fluctuations on past human societies have shifted towards the position that variability may be more important than change in shaping both biological and cultural adaptations. This shift is particularly apparent in the literature on human evolution, but is also reflected in studies of more recent periods as well as analyses of contemporary and future climates (e.g., Thornton et al. 2014; Vasseur et al. 2014; Seddon et al. 2016; Bathiany et al. 2018). It is widely understood that high-frequency fluctuations are more likely to govern adaptive dynamics and that, for example, cultural evolution becomes a more pervasive force when fluctuations occur rapidly relative to the generation time of the species concerned (e.g., Stephens 1991; Grove 2017). Yet despite this understanding definitions of climatic change and climatic variability are many and varied, with analyses often resting on subjective measures; it is clear that the intuitive but often implicit understanding of variability requires an objective, quantitative counterpart in order for the many valuable hypotheses regarding climatic variability to be rigorously tested, evaluated, and expanded.

Establishing a clear distinction between climatic change and climatic variability is particularly important from an evolutionary perspective, as these two components of climate can lead to distinct evolutionary responses. Whist climatic change often leads to directional selection or shifts in the geographic range of a species, climatic variability often leads to the evolution of various forms of phenotypic or behavioural plasticity. Evolutionary biologists have been aware of this distinction for decades (e.g. Dempster 1955; Levins 1968; Gillespie 1973; Moran 1992; Lande and Shannon 1996;

Simons 2002), and it has achieved even greater importance in the context of contemporary anthropogenic effects on global climates (e.g. Neukom et al. 2019). Species that have developed greater plasticity as a result of experiencing and adapting to temporal climatic variability are often more capable of dispersing into novel habitats (e.g. Mayr 1965; Vazquez 2006; Sol 2007), with important implications for conservation initiatives. The degree of environmental fluctuation has also been suggested to produce different macroscale evolutionary patterns, with gradual evolution more likely in relatively stable environments and punctuated equilibrium predominating under conditions of greater fluctuation (Sheldon 1996). This considerable body of literature is reviewed in greater detail in Grove (2015); in the present paper, it is sufficient to note that isolating climatic change from climatic variability will substantially enhance the potential for evolutionary analysis.

The CVD algorithm, detailed in Section 3, employs white noise as a quantitative model of variability. As white noise is stationary, lacks significant autocorrelation, and has high entropy, it fulfils all the necessary criteria for such a model. Crucially, white noise is fundamentally unpredictable, and as such it accords with the intuitive notion of variability that is adopted, implicitly or explicitly, by most researchers working with climatic time series. Although white noise by definition has equal power at all frequencies, its effects are most clearly manifest at high frequencies, where it stands out above the periodic or directional components that also regularly appear in climatic time series (see, for example, Figure 9).

The identification of white noise with variability allows for the construction of an algorithm that objectively decomposes a time series into change and variability components. Existing methods for performing such a decomposition require the analyst to make subjective choices of multiple parameter values; the CVD algorithm has only one free parameter, and the simulations of Section 4.4 demonstrate that varying this parameter has minimal effect on the result. The combination of non-parametric, data-adaptive SSA with more traditional Fourier-based methods obviates the need for computationally intensive simulation, resulting in a fast, efficient algorithm. As well as being valuable for the growing number of researchers studying the effects of climatic variability, this algorithm can also be employed as a 'de-noising' process by researchers focussing on the effects of longer-term trajectories. By way of demonstration, Section 5 presents a case study of a contemporary time series with the research focus on the change component, whereas Section 6 presents a case study of a prehistoric time series with a research focus on the variability component.

The extensive validation simulations of Section 4 demonstrate that the CVD algorithm is successful at recovering the variability and change components from a wide range of synthetic signals. Importantly, it isolates the variability component from a background that includes both periodic and red noise components, the two forms of fluctuation found most commonly in empirical climatic time series. The case studies of Sections 5 and 6 demonstrate that the decomposition of complex empirical climatic time series into change and variability components has the potential to produce genuine advances by isolating features of interest and facilitating more rigorous hypothesis testing.

Despite the numerous advantages of the CVD algorithm, a number of caveats must be noted. Some researchers may disagree with the view that variability and white noise should be viewed as synonymous. It is undoubtedly true that a proportion of the white noise identified via the algorithm will be instrumental, reflecting the precision with which a given proxy can be measured. However, in the vast majority of cases instrumental noise can be directly quantified (by, for example, repeatedly measuring the same sample and assessing the variance of the results). It is also clear from the case studies above that the amplitudes of white noise recovered far exceed those that could be produced via instrumental noise, and therefore that the vast majority of the white noise component represents true climatic variability.

The decomposition of a climatic time series into change and variability components does not explicitly address the issue of individual extreme events, but may be profitably combined with existing methods designed for the analysis of such events (a review of such methods is provided by Mudelsee 2014, Chapter 6). Individual events that temporally or permanently alter local climatic patterns (such as volcanic eruptions or tectonic shifts) may be recorded as alterations in either the change or variability components. The advantage of isolating these two components is that it will facilitate the identification of any effects caused by these events. For example, a temporary cooling caused by a 'volcanic winter' may be represented in the change component and, provided that the eruption is independently dated, this would allow researchers to investigate the consequences of that eruption in more detail. In a similar vein, tectonic events that alter the magnitude of a proxy – by, for example, diverting more runoff into a lake subject to coring for a precipitation record – should be recorded as a permanent change in the value of that proxy; any such change will be more apparent once the variability component of the time series has been removed.

The view that variability and white noise are synonymous permits the first objective, theoretically and mathematically grounded definition of variability as well as enabling the construction of an algorithm for its isolation; it is hoped that the white noise perspective will attract many users to the CVD algorithm, and will at least prompt debate among those who disagree with its theoretical foundations. A second caveat regards data quality, and is central to all studies of climatic time series. The SSA component of the algorithm requires time series equal in length to at least three times the period of the longest oscillatory fluctuation of interest; coverage of less than this threshold may lead to a less distinct separation of change and variability. Although SSA is the best solution for "short, noisy, chaotic signals" (Vautard et al. 1992:95), there are of course limits. Results generated via the CVD algorithm may be unreliable when signals are too short or are sampled at too low a resolution. In many cases, a beneficial approach to data collection may be to couple long, low-resolution signals with shorter, high-resolution sections of the same record (e.g., Lupien et al. 2020).

The case studies of Sections 5 and 6 indicate examples of how the CVD algorithm can be used, and are designed more as explications of the method than as definitive answers to the research questions they examine. In the future, more robust analyses using the algorithm could be generated by employing multiple time series that cover the same period and region but address different facets of climatic fluctuation. To take the case study of Section 6 as an example, the NGRIP and other Greenland cores also present dust (Ca^{2+}) and CO_2 data (e.g., Rasmussen et al. 2014), and the work of Bar-Matthews and colleagues (2003) suggests that the $\delta^{18}O$ and $\delta^{13}C$ records from the Soreq and Peqiin Cave speleothems, as well as organic carbon and *G. ruber* $\delta^{18}O$ records from eastern Mediterranean core MD84641 (Fontugne and Calvert 1992), provide in combination a fuller picture of palaeoclimatic fluctuations in southwest Asia across the period at which domestication first occurs. Whilst the high-variability phases of all these records would not necessarily be expected to align, they would in combination provide a more nuanced view of the different facets of variability during this important period.

The CVD algorithm allows researchers to decompose a time series into change and variability components, but this is merely a first step in the search for causal mechanisms or operational explanations. The analyses of Section 6, for example, establish the regional chronology of increases and decreases in variability and the relationship of this chronology to that of relevant archaeological records, but they do not delve into the finer-scale climatological patterns associated with these changes. For example, the amplitude and predictability of the seasonal cycle as well as the realised length of the growing season would have had profound consequences for the viability of agriculture. Faunal remains from Shubayqa 1 (Yeomans et al. 2017; Martin et al. 2016) suggest that winter

precipitation was declining and becoming more variable during the Late Natufian; the pollen record from Dor Lagoon (Kadosh et al. 2004) suggests a generally drier Late Natufian period followed by increased precipitation during the PPNA. It is important to note, however, that similar patterns of total annual precipitation can mask differences in the *distribution* of precipitation throughout the year. Geographically, Levantine precipitation decreases from west to east and from north to south, leading to substantial ecological variability within the region (Bar-Yosef 2011); the responses of different components of this ecological mosaic to varying longer-term fluctuations in precipitation would have been key to determining the feasibility of an agricultural mode of subsistence. Examining how patterns of seasonality interface with decadal and longer-term patterns of variability is a critical next step not only in terms of understanding the climatology but also in examining societal responses to regional and chronological variations.

Finally, the ability of the CVD algorithm to isolate the change and variability components of empirical time series may also prove useful in analysing contemporary climates and in forecasting their likely futures. The twin concerns of increasing variability (or increasing frequency of extremes) and global warming (e.g., Neukom et al. 2019) map clearly onto the variability and change components distinguished via the CVD algorithm, and it is of vital importance that their signatures are not conflated. Decomposing a time series into these two components not only allows researchers to analyse them separately, but also permits analysis of the relationships between them. In the terminal Pleistocene and Holocene NGRIP $\delta^{18}O$ record, for example, there is a clear association between cold, dry climates and higher variability; if contemporary climate records continue to reveal an association between warmer, wetter climates and higher variability then this shift in dynamics may be analysed further to provide insights into the nature of anthropogenic climate change. It is hoped that the CVD algorithm will therefore aid those studying the nature and effects of contemporary climate change as much as it will help those studying prehistoric human societies.

Acknowledgements

I would like to thank Martin Trauth, Anne Billingsley, Andy Cohen, Rachel Lupien, Rick Potts, James Blinkhorn, Lucy Timbrell, members of the UK and German Chew Bahir teams, and members of the Hominin Sites and Paleolakes Drilling Project for discussions of the issues tackled in this paper over many years. The comments of two anonymous reviewers both improved the manuscript and suggested numerous avenues for future research. This is publication #43 of the Hominin Sites and Paleolakes Drilling Project.

References

Aceituno, P., 1992. El Nino, the Southern Oscillation, and ENSO: Confusing names for a complex ocean atmosphere interaction. Bulletin of the American Meteorological Society 73, 483-485.

Allan, R.J., Lindesay, J., Parker, D., 1996. El Niño Southern Oscillation and Climatic Variability. CSIRO, Victoria.

Allan, R.J., Nicholls, N., Jones, P.D., Butterworth, I.J., 1991. A further extension of the Tahiti-Darwin SOI, early ENSE events and Darwin pressure. Journal of Climate 4, 743-749.

Allen, M.R., Robertson, A.W., 1996. Distinguishing modulated oscillations from coloured noise in multivariate datasets. Climate Dynamics 12, 775-784.

Allen, M.R., Smith, L.A., 1996. Monte Carlo SSA: Detecting irregular oscillations in the presence of colored noise. Journal of Climate 9, 3373-3404.

Andersen, K.K., Azuma, N., Barnola, J.M., Bigler, M., Biscaye, P., Caillon, N., Chappellaz, J., Clausen, H.B., DahlJensen, D., Fischer, H., Fluckiger, J., Fritzsche, D., Fujii, Y., Goto-Azuma, K., Gronvold, K., Gundestrup, N.S., Hansson, M., Huber, C., Hvidberg, C.S., Johnsen, S.J., Jonsell, U., Jouzel, J., Kipfstuhl, S., Landais, A., Leuenberger, M., Lorrain, R., Masson-Delmotte, V., Miller, H., Motoyama, H., Narita, H., Popp, T., Rasmussen, S.O., Raynaud, D., Rothlisberger, R., Ruth, U., Samyn, D., Schwander, J., Shoji, H., Siggard-Andersen, M.L., Steffensen, J.P., Stocker, T., Sveinbjornsdottir, A.E., Svensson, A., Takata, M., Tison, J.L., Thorsteinsson, T., Watanabe, O., Wilhelms, F., White, J.W.C., Project, N.G.I.C., 2004. High-resolution record of Northern Hemisphere climate extending into the last interglacial period. Nature 431, 147-151.

Arranz-Otaegui, A., Carretero, L.G., Ramsey, M.N., Fuller, D.Q., Richter, T., 2018. Archaeobotanical evidence reveals the origins of bread 14,400 years ago in northeastern Jordan. Proceedings of the National Academy of Sciences of the United States of America 115, 7925-7930.

Arranz-Otaegui, A., Carretero, L.G., Roe, J., Richter, T., 2018. "Founder crops" v. wild plants: Assessing the plant-based diet of the last hunter-gatherers in southwest Asia. Quaternary Science Reviews 186, 263-283.

Ashander, J., Chevin, L.M., Baskett, M.L., 2016. Predicting evolutionary rescue via evolving plasticity in stochastic environments. Proceedings of the Royal Society B-Biological Sciences 283.

Asouti, E., Fuller, D.Q., 2012. From foraging to farming in the southern Levant: the development of Epipalaeolithic and Pre-pottery Neolithic plant management strategies. Vegetation History and Archaeobotany 21, 149-162.

Bakun, A., Broad, K., 2003. Environmental 'loopholes' and fish population dynamics: comparative pattern recognition with focus on El Nino effects in the Pacific. Fisheries Oceanography 12, 458-473.

Barber, R.T., Chavez, F.P., 1983. Biological consequences of El Nino. Science 222, 1203-1210.

Bar-Matthews, M., Ayalon, A., Gilmour, M., Matthews, A., Hawkesworth, C.J., 2003. Sea-land oxygen isotopic relationships from planktonic foraminifera and speleothems in the Eastern Mediterranean region and their implication for paleorainfall during interglacial intervals. Geochimica Et Cosmochimica Acta 67, 3181-3199.

Bar-Matthews, M., Ayalon, A., Kaufman, A., 2000. Timing and hydrological conditions of Sapropel events in the Eastern Mediterranean, as evident from speleothems, Soreq cave, Israel. Chemical Geology 169, 145-156.

Bar-Matthews, M., Ayalon, A., Kaufman, A., Wasserburg, G.J., 1999. The Eastern Mediterranean paleoclimate as a reflection of regional events: Soreq cave, Israel. Earth and Planetary Science Letters 166, 85-95.

Bar-Yosef, O., 1998. The Natufian culture in the Levant, threshold to the origins of agriculture. Evolutionary Anthropology 6, 159-177.

Bar-Yosef, O., 2011. Climatic Fluctuations and Early Farming in West and East Asia. Current Anthropology, 52, S175-S193. doi:10.1086/659784

Bar-Yosef, O., Belfer-Cohen, A., 1992. From foraging to farming in the Mediterranean Levant, in: Gebauer, A.B., Price, T.D. (Eds.), Transitions to Agriculture in Prehistory. Prehistory Press, Madison.

Bar-Yosef, O., Belfer-Cohen, A., 2002. Facing environmental crisis: societal and cultural changes at the transition from the Younger Dryas to the Holocene in the Levant, in: Cappers, R.T.J., Bottema, S. (Eds.), The Dawn of Farming in the Near East. Ex Oriente, Berlin.

Barzilai, O., Rebollo, N., Nadel, D., Bocquentin, F., Yeshurun, R., Lengyel, G., Bermatov-Paz, G., Boaretto, E., 2017. Radiocarbon dating of human burials from Raqefet Cave and contemporaneous Natufian traditions at Mount Carmel. Antiquity 91, 1137-1154.

Bathiany, S., Dakos, V., Scheffer, M., Lenton, T.M., 2018. Climate models predict increasing temperature variability in poor countries. Science Advances 4.

Bettinger, R., Richerson, P., Boyd, R., 2009. Constraints on the Development of Agriculture. Current Anthropology 50, 627-631.

Betts, R.A., Jones, C.D., Knight, J.R., Keeling, R.F., Kennedy, J.J., 2016. El Nino and a record CO2 rise. Nature Climate Change 6, 806-810.

Blockley, S.P.E., Pinhasi, R., 2011. A revised chronology for the adoption of agriculture in the Southern Levant and the role of Lateglacial climatic change. Quaternary Science Reviews 30, 98-108.

Bloomfield, P., 2000. Fourier Analysis of Time Series. Wiley, New York.

Braidwood, R.J., 1960. The agricultural revolution. Scientific American 203, 130-&.

Braidwood, R.J., Braidwood, L., 1953. The Earliest Village Communities of Southwest Asia. Journal of World History 1, 278-310.

Braidwood, R.J., Howe, B., 1960. Prehistoric Investigations in Iraqi Kurdistan. University of Chicago Press (Oriental Institute), Chicago.

Broomhead, D.S., King, G.P., 1986. Extracting qualitative dynamics from experimental data. Physica D 20, 217-236.

Burroughs, W.J., 2005. Climate Change in Prehistory: The End of The Reign of Chaos. Cambridge University Press, Cambridge.

Caracuta, V., Weinstein-Evron, M., Yeshurun, R., Kaufman, D., Tsatskin, A., Boaretto, E., 2016. Charred wood remains in the natufian sequence of el-Wad terrace (Israel): New insights into the climatic, environmental and cultural changes at the end of the Pleistocene. Quaternary Science Reviews 131, 20-32.

Chatfield, C., 1989. The analysis of time series: theory and practice (4th ed.). Chapman and Hall, London.

Chen, Y., Morton, D.C., Andela, N., van der Werf, G.R., Giglio, L., Randerson, J.T., 2017. A pan-tropical cascade of fire driven by El Nino/Southern Oscillation. Nature Climate Change 7, 906-+.

Chevin, L.M., Cotto, O., Ashander, J., 2017. Stochastic Evolutionary Demography under a Fluctuating Optimum Phenotype. American Naturalist 190, 786-802.

Childe, V.G., 1928. The Most Ancient East. Kegan Paul, London.

Chon, K.H., Scully, C.G., Lu, S., 2009. Approximate Entropy for all Signals Is the Recommended Threshold Value r Appropriate? Ieee Engineering in Medicine and Biology Magazine 28, 18-23.

Cohen, D., 1966. Optimizing reproduction in a randomly varying environment. Journal of Theoretical Biology 12, 119-&.

Cox, P.M., Pearson, D., Booth, B.B., Friedlingstein, P., Huntingford, C., Jones, C.D., Luke, C.M., 2013. Sensitivity of tropical carbon to climate change constrained by carbon dioxide variability. Nature 494, 341-344.

Cuddington, K.M., Yodzis, P., 1999. Black noise and population persistence. Proceedings of the Royal Society B-Biological Sciences 266, 969-973.

Dart, R.A., 1925. Australopithecus africanus: the man-ape of South Africa. Nature 115, 195-199.

Dart, R.A., 1953. The predatory transition from ape to man. International Anthropology and Linguistics Review 1, 201-2018.

Delgado-Bonal, A., 2019. Quantifying the randomness of the stock markets. Scientific Reports 9.

Delgado-Bonal, A., 2020. On the use of complexity algorithms: a cautionary lesson from climate research. Scientific Reports 10.

Delgado-Bonal, A., Marshak, A., 2019. Approximate Entropy and Sample Entropy: A Comprehensive Tutorial. Entropy 21.

Dempster, E.R., 1955. Maintenance of genetic heterogeneity. Cold Spring Harbor Symposia on Quantitative Biology 20, 25-32.

Ditlevsen, P.D., Svensmark, H., Johnsen, S., 1996. Contrasting atmospheric and climate dynamics of the last-glacial and Holocene periods. Nature 379, 810-812.

Fadlallah, B., Chen, B.D., Keil, A., Principe, J., 2013. Weighted-permutation entropy: A complexity measure for time series incorporating amplitude information. Physical Review E 87.

Fama, E.F., 1970. Efficient capital markets: review of theory and empirical work. Journal of Finance 25, 383-423.

Fama, E.F., 1991. Efficient capital markets 2. Journal of Finance 46, 1575-1617.

Feynman, J., Ruzmaikin, A., 2007. Climate stability and the development of agricultural societies. Climatic Change 84, 295-311.

Flannery, K.V., 1969. Origins and ecological effects of early domestication in Iran and the Near East, in: Ucko, P., Dimbleby, G. (Eds.), The Domestication and Exploitation of Plants and Animals. Duckworth, London, pp. 73-100.

Fontugne, M.R., Calvert, S.E., 1992. Late Pleistocene variability of the carbon isotopic composition of organic matter in the eastern Mediterranean: monitor of changes in carbon sources and atmospheric CO2 concentrations. Paleoceanography 7, 1-20.

Fuller, D.Q., Denham, T., Arroyo-Kalin, M., Lucas, L., Stevens, C.J., Qin, L., Allaby, R.G., Purugganan, M.D., 2014. Convergent evolution and parallelism in plant domestication revealed by an expanding archaeological record. Proceedings of the National Academy of Sciences of the United States of America 111, 6147-6152.

Fuller, D.Q., Willcox, G., Allaby, R.G., 2012. Early agricultural pathways: moving outside the 'core area' hypothesis in Southwest Asia. Journal of Experimental Botany 63, 617-633.

Garland, J., James, R., Bradley, E., 2014. Model-free quantification of time-series predictability. Physical Review E 90.

Ghil, M., Allen, M.R., Dettinger, M.D., Ide, K., Kondrashov, D., Mann, M.E., Robertson, A.W., Saunders, A., Tian, Y., Varadi, F., Yiou, P., 2002. Advanced spectral methods for climatic time series. Reviews of Geophysics 40.

Gillespie, J., 1973. Polymorphism in random environments. Theoretical Population Biology 4, 193-195.

Gilman, D.L., Fuglister, F.J., Mitchell, J.M., 1963. On the power spectrum of red noise. Journal of the Atmospheric Sciences 20, 182-184.

Glantz, M.H., 1996. Currents of Change: El Nino's Impact on Climate and Society. Cambridge University Press, Cambridge.

Golyandina, N., Nekrutkin, V., Zhigljavsky, A., 2001. Analysis of Time Series Structure: SSA and related techniques. Chapman and Hall, London.

Golyandina, N., Zhigljavsky, A., 2013. Singular Spectrum Analysis for Time Series. Springer, Berlin.

Goring-Morris, N., Belfer-Cohen, A., 1997. The articulation of cultural processes and Late Quaternary environmental changes in Cisjordan. Paleorient 23, 71-93.

Grant, P.R., Grant, B.R., Keller, L.F., Petren, K., 2000. Effects of El Nino events on Darwin's finch productivity. Ecology 81, 2442-2457.

Grootes, P.M., Stuiver, M., 1997. Oxygen 18/16 variability in Greenland snow and ice with 10(-3)- to 10(5)-year time resolution. Journal of Geophysical Research-Oceans 102, 26455-26470.

Grosman, L., 2013. The Natufian Chronological Scheme: New Insights and their Implications, in: Bar-Yosef, O., Valla, F.R. (Eds.), Natufian Foragers in the Levant: Terminal Pleistocene Social Changes in Western Asia. Berghahn Books, New York, pp. 622-627.

Groth, A., Ghil, M., 2015. Monte Carlo Singular Spectrum Analysis (SSA) Revisited: Detecting Oscillator Clusters in Multivariate Datasets. Journal of Climate 28, 7873-7893.

Grove, M., 2011a. Speciation, diversity, and Mode 1 technologies: The impact of variability selection. Journal of Human Evolution 61, 306-319.

Grove, M., 2011b. Change and variability in Plio-Pleistocene climates: modelling the hominin response. Journal of Archaeological Science 38, 3038-3047.

Grove, M., 2015. Palaeoclimates, plasticity, and the early dispersal of Homo sapiens. Quaternary International 369, 17-37.

Grove, M., 2017. Environmental complexity, life history, and encephalisation in human evolution. Biology & Philosophy 32, 395-420.

Grove, M., Borg, J.M., Pollack, F., 2020. Coloured noise time series as appropriate models for environmental variation in artificial evolutionary systems. ALIFE 2020, 292-299.

Haldane, J.B.S., Jayakar, S.D., 1962. Polymorphism due to selection of varying direction. Journal of Genetics 58, 237-&.

Halley, J.M., 1996. Ecology, evolution and 1/f-noise. Trends in Ecology & Evolution 11, 33-37.

Halley, J.M., Inchausti, P., 2004. The increasing importance of 1/f-noises as models of ecological variability. Fluctuation and Noise Letters 4, R1-R26.

Halley, J.M., Kunin, V.E., 1999. Extinction risk and the 1/f family of noise models. Theoretical Population Biology 56, 215-230.

Hastings, H.M., Sugihara, G., 1993. Fractals: A User's Guide for the Natural Sciences. Oxford University Press, Oxford.

Henry, D.O., 1989. From Foraging to Agriculture: the Levant at the End of the Ice Age. University of Pennsylvania Press, Philadelphia.

Henry, D.O., 1995. The Natufian Sites and the Emergence of Complex Foraging, in: Henry, D.O. (Ed.), Prehistoric Cultural Ecology and Evolution: Insights from Southern Jordan. Plenum Press, New York, pp. 319-335.

Henry, D.O., 2013. The Natufian and the Younger Dryas, in: Bar-Yosef, O., Valla, F.R. (Eds.), Natufian Foragers in the Levant. International Monographs in Prehistory, Ann Arbor, pp. 584-610.

Hillman, G.C., 1996. Late Pleistocene changes in wild plant foods available to hunter-gatherers of the northern Fertil Crescent: possible preludes to cereal cultivation, in: Harris, D.R. (Ed.), The Origins and Spread of Agriculture and Pastoralism in Eurasia. UCL Press, London, pp. 159-203.

Humphrey, V., Zscheischler, J., Ciais, P., Gudmundsson, L., Sitch, S., Seneviratne, S.I., 2018. Sensitivity of atmospheric CO2 growth rate to observed changes in terrestrial water storage. Nature 560, 628-+.

Inchausti, P., Halley, J., 2001. Investigating long-term ecological variability using the global population dynamics database. Science 293, 655-657.

Jaksic, F.M., 2001. Ecological effects of El Nino in terrestrial ecosystems of western South America. Ecography 24, 241-250.

Jenkins, G.M., Watts, D.G., 1968. Spectral Analysis and its Applications. Holden-Day, San Francisco.

Johnsen, S.J., Clausen, H.B., Dansgaard, W., Gundestrup, N.S., Hammer, C.U., Andersen, U., Andersen, K.K., Hvidberg, C.S., DahlJensen, D., Steffensen, J.P., Shoji, H., Sveinbjornsdottir, A.E., White, J., Jouzel, J., Fisher, D., 1997. The delta O-18 record along the Greenland Ice Core Project deep ice core and the problem of possible Eemian climatic instability. Journal of Geophysical Research-Oceans 102, 26397-26410.

Kadosh, D., Sivan, D., Kutiel, H., Weinstein-Evron, M., 2004. A Late quaternary paleoenvironmental sequence from Dor, Carmel coastal plain, Israel. Palynology 28, 143-157.

Kasdin, N.J., 1995. Discrete simulation of colored noise and stochastic processes and 1/f power-law noise generation. Proceedings of the Ieee 83, 802-827.

Keppenne, C.L., Ghil, M., 1992. Adaptive filtering and prediction of the Southern Oscillation Index. Journal of Geophysical Research-Atmospheres 97, 20449-20454.

Keshner, M.S., 1982. 1/f noise. Proceedings of the Ieee 70, 212-218.

Kiladis, G.N., Van Loon, H., 1988. The Southern Oscillation. VII. Meteorological anomalies over the Indian and Pacific sectors associated with the extremes of the oscillation. Monthly Weather Review 116, 120-136.

Kingston, J.D., 2007. Shifting Adaptive Landscapes: Progress and Challenges in Reconstructing Early Hominid Environments, in: Stinson, S. (Ed.), Yearbook of Physical Anthropology, Vol 50, pp. 20-58.

Kingston, J.D., Deino, A.L., Edgar, R.K., Hill, A., 2007. Astronomically forced climate change in the Kenyan Rift Valley 2.7-2.55 Ma: implications for the evolution of early hominin ecosystems. Journal of Human Evolution 53, 487-503.

Kingston, J.D., Harrison, T., 2007. Isotopic dietary reconstructions of Pliocene herbivores at Laetoli: implications for early hominin paleoecology. . Palaeogeography, Palaeoclimatology, Palaeoecology 243, 272-306.

Lande, R., Shannon, S., 1996. The role of genetic variation in adaptation and population persistence in a changing environment. Evolution 50, 434-437.

Larkin, N.K., Harrison, D.E., 2005. On the definition of El Nino and associated seasonal average US weather anomalies. Geophysical Research Letters 32.

Larson, G., Piperno, D.R., Allaby, R.G., Purugganan, M.D., Andersson, L., Arroyo-Kalin, M., Barton, L., Vigueira, C.C., Denham, T., Dobney, K., Doust, A.N., Gepts, P., Gilbert, M.T.P., Gremillion, K.J., Lucas, L., Lukens, L., Marshall, F.B., Olsen, K.M., Pires, J.C., Richerson, P.J., de Casas, R.R., Sanjur, O.I., Thomas, M.G., Fuller, D.Q., 2014. Current perspectives and the future of domestication studies. Proceedings of the National Academy of Sciences of the United States of America 111, 6139-6146.

Lee, M.S.Y., Doughty, P., 2003. The geometric meaning of macroevolution. Trends in Ecology & Evolution 18, 263-266.

Letnic, M., Tamayo, B., Dickman, C.R., 2005. The responses of mammals to La Nina (El Nino Southern Oscillation)-associated rainfall, predation, and wildfire in central Australia. Journal of Mammalogy 86, 689-703.

Levene, H., 1953. Genetic equilibrium when more than one ecological niche is available. American Naturalist 87, 331-333.

Levins, R., 1968. Evolution in changing environments. Princeton University Press, Princeton.

Lewontin, R.C., Cohen, D., 1969. On population growth in a randomly varying environment. Proceedings of the National Academy of Sciences of the United States of America 62, 1056-&.

Lim, K.P., Brooks, R., 2011. The evolution of stock market efficiency over time: a survey of the empirical literature. Journal of Economic Surveys 25, 69-108.

Liu, J.J., Bowman, K.W., Schimel, D.S., Parazoo, N.C., Jiang, Z., Lee, M., Bloom, A.A., Wunch, D., Frankenberg, C., Sun, Y., O'Dell, C.W., Gurney, K.R., Menemenlis, D., Gierach, M., Crisp, D., Eldering, A., 2017. Contrasting carbon cycle responses of the tropical continents to the 2015-2016 El Nino. Science 358.

Lovejoy, S., Schertzer, D., 1986. Scale-invariance in climatological temperatures and the local spectral plateau. Annales Geophysicae Series B-Terrestrial and Planetary Physics 4, 401-409.

Lupien, R.L., Russell, J.M., Grove, M., Beck, C.C., Feibel, C.S., Cohen, A.S., 2020. Abrupt climate change and its influences on hominin evolution during the early Pleistocene in the Turkana Basin, Kenya. Quaternary Science Reviews 245.

Maeda, O., Lucas, L., Silva, F., Tanno, K.I., Fuller, D.Q., 2016. Narrowing the harvest: Increasing sickle investment and the rise of domesticated cereal agriculture in the Fertile Crescent. Quaternary Science Reviews 145, 226-237.

Mandelbrot, B., Wallis, J.R., 1969. Some long-run properties of geophysical records. Water Resources Research 5, 321-&.

Martin, L., Edwards, Y. H., Roe, J., Garrard, A., 2016. Faunal turnover in the Azraq Basin, eastern Jordan 28,000 to 9000 cal yr BP, signalling climate change and human impact. Quaternary Research 86(2), 200-219. doi:10.1016/j.yqres.2016.07.001

Maslin, M.A., Brierley, C.M., Milner, A.M., Shultz, S., Trauth, M.H., Wilson, K.E., 2014. East African climate pulses and early human evolution. Quaternary Science Reviews 101, 1-17.

Maslin, M.A., Trauth, M.H., 2009. Plio-Pleistocene East African Pulsed Climate Variability and Its Influence on Early Human Evolution, in: Grine, F.E., Fleagle, J.G., Leakey, R.E. (Eds.), The First Humans: Origin and Early Evolution of the Genus Homo. Springer, New York, pp. 151-158.

Mayr, E., 1965. The nature of colonizations in birds. In H. G. Baker & G. L. Stebbins (Eds.), The Genetics of Colonizing Species (pp. 29-43). London: Academic Press.

McKillup, S.C., McKillup, R.V., 1997. An outbreak of the moth Achaea serva (Fabr) on the mangrove Excoecaria agallocha (L). Pan-Pacific Entomologist 73, 184-185.

Milner, A.M., Collier, R.E.L., Roucoux, K.H., Muller, U.C., Pross, J., Kalaitzidis, S., Christanis, K., Tzedakis, P.C., 2012. Enhanced seasonality of precipitation in the Mediterranean during the early part of the Last Interglacial. Geology 40, 919-922.

Milner, A.M., Muller, U.C., Roucoux, K.H., Collier, R.E.L., Pross, J., Kalaitzidis, S., Christanis, K., Tzedakis, P.C., 2013. Environmental variability during the Last Interglacial: a new high-resolution pollen record from Tenaghi Philippon, Greece. Journal of Quaternary Science 28, 113-117.

Milner, A.M., Roucoux, K.H., Collier, R.E.L., Muller, U.C., Pross, J., Tzedakis, P.C., 2016. Vegetation responses to abrupt climatic changes during the Last Interglacial Complex (Marine Isotope Stage 5) at Tenaghi Philippon, NE Greece. Quaternary Science Reviews 154, 169-181.

Moore, A.M.T., Hillman, G.C., 1992. The Pleistocene to Holocene transition and human economy in southwest Asia: the impact of the Younger Dryas. American Antiquity 57, 482-494.

Moran, N.A., 1992. The evolutionary maintenance of alternative phenotypes. American Naturalist 139, 971-989.

Mudelsee, M., 2014. Climate Time Series Analysis: Classical Statistical and Bootstrap Methods. Springer, Geneva.

Munro, N.D., 2004. Zooarchaeological measures of hunting pressure and occupation intensity in the Natufian - Implications for agricultural origins. Current Anthropology 45, S5-S33.

Neukom, R., Barboza, L.A., Erb, M.P., Shi, F., Emile-Geay, J., Evans, M.N., Franke, J., Kaufman, D.S., Lucke, L., Rehfeld, K., Schurer, A., Zhu, F., Bronnimann, S., Hakim, G.J., Henley, B.J., Ljungqvist, F.C., McKay, N., Valler, V., von Gunten, L., Pages 2k, C., 2019. Consistent multidecadal variability in global temperature reconstructions and simulations over the Common Era. Nature Geoscience 12, 643-+.

Nicholson, S.E., Selato, J.C., 2000. The influence of La Nina on African rainfall. International Journal of Climatology 20, 1761-1776.

Pelletier, J.D., 1997. Analysis and modeling of the natural variability of climate. Journal of Climate 10, 1331-1342.

Pielke, R. A., 2004. What is climate change? Issues in Science and Technology 20, 31-34.

Pincus, S., 1995. Approximate entropy (ApEn) as a complexity measure. Chaos 5, 110-117.

Pincus, S., 2008. Approximate entropy as an irregularity measure for financial data. Econometric Reviews 27, 329-362.

Pincus, S., Kalman, R.E., 2004. Irregularity, volatility, risk, and financial market time series. Proceedings of the National Academy of Sciences of the United States of America 101, 13709-13714.

Pincus, S., Singer, B.H., 1998. A recipe for randomness. Proceedings of the National Academy of Sciences of the United States of America 95, 10367-10372.

Pincus, S.M., 1991. Approximate entropy as a measure of system complexity. Proceedings of the National Academy of Sciences of the United States of America 88, 2297-2301.

Piperno, D.R., Weiss, E., Holst, I., Nadel, D., 2004. Processing of wild cereal grains in the Upper Palaeolithic revealed by starch grain analysis. Nature 430, 670-673.

Polis, G.A., Hurd, S.D., Jackson, C.T., Pinero, F.S., 1997. El Nino effects on the dynamics and control of an island ecosystem in the Gulf of California. Ecology 78, 1884-1897.

Potts, R., 1996a. Humanity's Descent: The Consequences of Ecological Instability. William Morrow, New York.

Potts, R., 1996b. Evolution and climate variability. Science 273, 922-923.

Potts, R., 1998a. Variability selection in hominid evolution. Evolutionary Anthropology 7, 81-96.

Potts, R., 1998b. Environmental hypotheses of hominin evolution, in: Ruff, C. (Ed.), Yearbook of Physical Anthropology, Vol 41 - 1998, pp. 93-136.

Potts, R., 2012. Evolution and Environmental Change in Early Human Prehistory, in: Brenneis, D., Ellison, P.T. (Eds.), Annual Review of Anthropology, Vol 41, pp. 151-167.

Potts, R., 2013. Hominin evolution in settings of strong environmental variability. Quaternary Science Reviews 73, 1-13.

Potts, R., Behrensmeyer, A.K., Faith, J.T., Tryon, C.A., Brooks, A.S., Yellen, J.E., Deino, M.L., Kinyanjui, R., Clark, J.B., Haradon, C.M., Levin, N.E., Meijer, H.J.M., Veatch, E.G., Owen, R.B., Renaut, R.W., 2018. Environmental dynamics during the onset of the Middle Stone Age in eastern Africa. Science 360, 86-+.

Potts, R., Dommain, R., Moerman, J.W., Behrensmeyer, A.K., Deino, A.L., Riedl, S., Beverly, E.J., Brown, E.T., Deocampo, D., Kinyanjui, R., Lupien, R., Owen, R.B., Rabideaux, N., Russell, J.M., Stockhecke, M., DeMenocal, P., Faith, J.T., Garcin, Y., Noren, A., Scott, J.J., Western, D., Bright, J., Clark, J.B., Cohen, A.S., Keller, C.B., King, J., Levin, N.E., Shannon, K.B., Muiruri, V., Renaut, R.W., Rucina, S.M., Uno, K., 2020. Increased ecological resource variability during a critical transition in hominin evolution. Science Advances 6.

Potts, R., Faith, J.T., 2015. Alternating high and low climate variability: The context of natural selection and speciation in Plio-Pleistocene hominin evolution. Journal of Human Evolution 87, 5-20.

Power, S., Casey, T., Folland, C., Colman, A., Mehta, V., 1999. Inter-decadal modulation of the impact of ENSO on Australia. Climate Dynamics 15, 319-324.

Press, W.H., 1978. Flicker noises in astronomy and elsewhere. Comments in Astrophysics 7, 103-119.

Priestley, 1981. Spectral Analysis and Time Series. Academic Press, London.

Rasmussen, S.O., Andersen, K.K., Svensson, A.M., Steffensen, J.P., Vinther, B.M., Clausen, H.B., Siggaard-Andersen, M.L., Johnsen, S.J., Larsen, L.B., Dahl-Jensen, D., Bigler, M., Rothlisberger, R., Fischer, H., Goto-Azuma, K., Hansson, M.E., Ruth, U., 2006. A new Greenland ice core chronology for the last glacial termination. Journal of Geophysical Research-Atmospheres 111.

Rasmussen, S.O., Bigler, M., Blockley, S.P., Blunier, T., Buchardt, S.L., Clausen, H.B., Cvijanovic, I., Dahl-Jensen, D., Johnsen, S.J., Fischer, H., Gkinis, V., Guillevic, M., Hoek, W.Z., Lowe, J.J., Pedro, J.B., Popp, T., Seierstad, I.K., Steffensen, J.P., Svensson, A.M., Vallelonga, P., Vinther, B.M., Walker, M.J.C., Wheatley, J.J., Winstrup, M., 2014. A stratigraphic framework for abrupt climatic changes during the Last Glacial period based on three synchronized Greenland ice-core records: refining and extending the INTIMATE event stratigraphy. Quaternary Science Reviews 106, 14-28.

Richerson, P.J., Boyd, R., Bettinger, R.L., 2001. Was agriculture impossible during the Pleistocene but mandatory during the Holocene? A climate change hypothesis. American Antiquity 66, 387-411.

Richter, T., Arranz-Otaegui, A., Yeomans, L., Boaretto, E., 2017. High Resolution AMS Dates from Shubayqa 1, northeast Jordan Reveal Complex Origins of Late Epipalaeolithic Natufian in the Levant. Scientific Reports 7.

Roberts, N., Woodbridge, J., Bevan, A., Palmisano, A., Shennan, S., Asouti, E., 2018. Human responses and non-responses to climatic variations during the last Glacial-Interglacial transition in the eastern Mediterranean. Quaternary Science Reviews 184, 47-67.

Robinson, J.T., 1954. Prehominid dentition and hominid evolution. Evolution 8, 324-334.

Robinson, S.A., Black, S., Sellwood, B.W., Valdes, P.J., 2006. A review of palaeoclimates and palaeoenvironments in the Levant and Eastern Mediterranean from 25,000 to 5000 years BP: setting the environmental background for the evolution of human civilisation. Quaternary Science Reviews 25, 1517-1541.

Ropelewski, C.F., Jones, P.D., 1987. An extension of the Tahiti-Darwin Southern Oscillation Index. Monthly Weather Review 115, 2161-2165.

Rosen, A.M., 2010. Natufian plant exploitation: managing risk and stability in an environment of change. Eurasian Prehistory 7, 113-127.

Rosen, A.M., Rivera-Collazo, I., 2012. Climate change, adaptive cycles, and the persistence of foraging economies during the late Pleistocene/Holocene transition in the Levant. Proceedings of the National Academy of Sciences of the United States of America 109, 3640-3645.

Sadori, L., Koutsodendris, A., Panagiotopoulos, K., Masi, A., Bertini, A., Combourieu-Nebout, N., Francke, A., Kouli, K., Joannin, S., Mercuri, A.M., Peyron, O., Torri, P., Wagner, B., Zanchetta, G., Sinopoli, G., Donders, T.H., 2016. Pollen-based paleoenvironmental and paleoclimatic change at Lake Ohrid (south-eastern Europe) during the past 500 ka. Biogeosciences 13, 1423-1437.

Saupe, D., 1988. Algorithms for random fractals, in: Peitgen, H.O., Saupe, D. (Eds.), The Science of Fractal Images. Springer, New York, pp. 71-136.

Seddon, A.W.R., Macias-Fauria, M., Long, P.R., Benz, D., Willis, K.J., 2016. Sensitivity of global terrestrial ecosystems to climate variability. Nature 531, 229-+.

Seierstad, I.K., Abbott, P.M., Bigler, M., Blunier, T., Bourne, A.J., Brook, E., Buchardt, S.L., Buizert, C., Clausen, H.B., Cook, E., Dahl-Jensen, D., Davies, S.M., Guillevic, M., Johnsen, S.J., Pedersen, D.S., Popp, T.J., Rasmussen, S.O., Severinghaus, J.P., Svensson, A., Vinther, B.M., 2014. Consistently dated records from the Greenland GRIP, GISP2 and NGRIP ice cores for the past 104 ka reveal regional millennial-scale delta O-18 gradients with possible Heinrich event imprint. Quaternary Science Reviews 106, 29-46.

Sheldon, P. R., 1996. Plus ca change - A model for stasis and evolution in different environments. Palaeogeography Palaeoclimatology Palaeoecology 127, 209-227. doi:10.1016/s0031-0182(96)00096-x

Simons, A.M., 2002. The continuity of microevolution and macroevolution. Journal of Evolutionary Biology 15, 688-701.

Sinopoli, G., Masi, A., Regattieri, E., Wagner, B., Francke, A., Peyron, O., Sadori, L., 2018. Palynology of the Last Interglacial Complex at Lake Ohrid: palaeoenvironmental and palaeoclimatic inferences. Quaternary Science Reviews 180, 177-192.

Smith, C.A., Sardeshmukh, P.D., 2000. The effect of ENSO on the intraseasonal variance of surface temperatures in winter. International Journal of Climatology 20, 1543-1557.

Snir, A., Nadel, D., Groman-Yaroslavski, I., Melamed, Y., Sternberg, M., Bar-Yosef, O., Weiss, E., 2015. The Origin of Cultivation and Proto-Weeds, Long Before Neolithic Farming. Plos One 10.

Sol, D., 2007. Do successful invaders exist? Pre-adaptations to novel environments in terrestrial vertebrates. In W. Nentwig (Ed.), Biological Invasions (pp. 127-141). Berlin: Springer-Verlag.

Stephens, D.W., 1991. Change, regularity, and value in the evolution of animal learning. Behavioral Ecology 2, 77-89.

Stuiver, M., Grootes, P.M., 2000. GISP2 oxygen isotope ratios. Quaternary Research 53, 277-283.

Thornton, P.K., Ericksen, P.J., Herrero, M., Challinor, A.J., 2014. Climate variability and vulnerability to climate change: a review. Global Change Biology 20, 3313-3328.

Tian, H.Q., Melillo, J.M., Kicklighter, D.W., McGuire, A.D., Helfrich, J.V.K., Moore, B., Vorosmarty, C.J., 1998. Effect of interannual climate variability on carbon storage in Amazonian ecosystems. Nature 396, 664-667.

Torrence, C., Compo, G.P., 1998. A practical guide to wavelet analysis. Bulletin of the American Meteorological Society 79, 61-78.

Trauth, M.H., 2015. Matlab Recipes for Earth Sciences (4th Ed). Springer, Berlin.

Trauth, M.H., Larrasoana, J.C., Mudelsee, M., 2009. Trends, rhythms and events in Plio-Pleistocene African climate. Quaternary Science Reviews 28, 399-411.

Trauth, M.H., Maslin, M.A., Deino, A.L., Junginger, A., Lesoloyia, M., Odada, E.O., Olago, D.O., Olaka, L.A., Strecker, M.R., Tiedemann, R., 2010. Human evolution in a variable environment: the amplifier lakes of Eastern Africa. Quaternary Science Reviews 29, 2981-2988.

Trenberth, K.E., 1997. The definition of El Nino. Bulletin of the American Meteorological Society 78, 2771-2777.

Vaks, A., Bar-Matthews, M., Ayalon, A., Matthews, A., Frumkin, A., Dayan, U., Halicz, L., Almogi-Labin, A., Schilman, B., 2006. Paleoclimate and location of the border between Mediterranean climate region and the Saharo-Arabian Desert as revealed by speleothems from the northern Negev Desert, Israel. Earth and Planetary Science Letters 249, 384-399.

Vanzeist, W., Wright, H.E., 1963. Preliminary pollen studies at Lake Zeribar, Zagros Mountains, southwestern Iran. Science 140, 65-&.

Vasseur, D.A., DeLong, J.P., Gilbert, B., Greig, H.S., Harley, C.D.G., McCann, K.S., Savage, V., Tunney, T.D., O'Connor, M.I., 2014. Increased temperature variation poses a greater risk to species than climate warming. Proceedings of the Royal Society B-Biological Sciences 281.

Vaughan, S., 2005. A simple test for periodic signals in red noise. Astronomy & Astrophysics 431, 391-403.

Vautard, R., Ghil, M., 1989. Singular spectrum analysis in nonlinear dynamics, with applications to paleoclimatic time series. Physica D 35, 395-424.

Vautard, R., Yiou, P., Ghil, M., 1992. Singular spectrum analysis: a toolkit for short, noisy chaotic signals. Physica D 58, 95-126.

Vazquez, D. P., 2006. Exploring the relationship between niche breadth and invasion success. In M. W. Cadotte (Ed.), Conceptual Ecology and Invasion Biology (pp. 307-322). Dordrecht: Springer.

Vecchi, G.A., Soden, B.J., Wittenberg, A.T., Held, I.M., Leetmaa, A., Harrison, M.J., 2006. Weakening of tropical Pacific atmospheric circulation due to anthropogenic forcing. Nature 441, 73-76.

Voss, R.F., 1988. Fractals in nature: From characterization to simulation, in: Peitgen, H.O., Saupe, D. (Eds.), The Science of Fractal Images. Springer, New York, pp. 21-70.

Washburn, S.L., 1960. Tools and human evolution. Scientific American 203, 63-75.

Weiss, E., Zohary, D., 2011. The Neolithic Southwest Asian Founder Crops Their Biology and Archaeobotany. Current Anthropology 52, S237-S254.

Wright, H.E., 1968. Natural environment of early food production north of Mesopotamia. Science 161, 334-&.

Wright, H.E., 1976. Environmental setting for plant domestication in Near East. Science 194, 385-389.

Wright, H.E., 1993. Environmental determinism in Near Eastern prehistory. Current Anthropology 34, 458-469.

Wright, S.J., Carrasco, C., Calderon, O., Paton, S., 1999. The El Nino Southern Oscillation variable fruit production, and famine in a tropical forest. Ecology 80, 1632-1647.

Wulf, S., Hardiman, M.J., Staff, R.A., Koutsodendris, A., Appelt, O., Blockley, S.P.E., Lowe, J., Manning, C.J., Ottolini, L., Schmitt, A.K., Smith, V.C., Tomlinson, E.L., Vakhrameeva, P., Knipping, M., Kotthoff, U., Milner, A.M., Muller, U.C., Christanis, K., Kalaitzidis, S., Tzedakis, P.C., Schmiedl, G., Pross, J., 2018. The marine isotope stage 1-5 cryptotephra record of Tenaghi Philippon, Greece: Towards a detailed tephrostratigraphic framework for the Eastern Mediterranean region. Quaternary Science Reviews 186, 236-262.

Yeomans, L., Richter, T., & Martin, L., 2017. Environment, seasonality and hunting strategies as influences on Natufian food procurement: The faunal remains from Shubayqa 1. Levant 49, 85-104. doi:10.1080/00758914.2017.1368820

Figures

Figure 1. Simulated time series demonstrating some of the difficulties of distinguishing between change and variability. See text for further details.

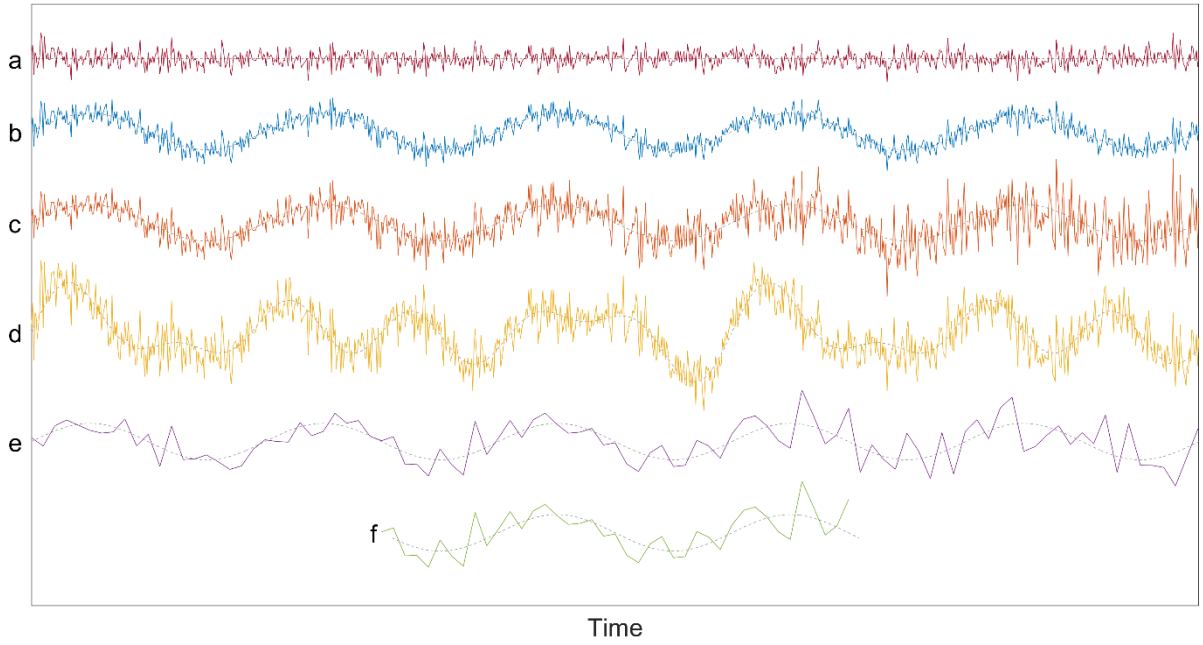

Figure 2. a) a simulated time series with two examples of Gaussian smoothing. b) and c) show the estimates of variability produced by detrending the original time series by the two smoothing examples. d) shows the differences between these two estimates of variability.

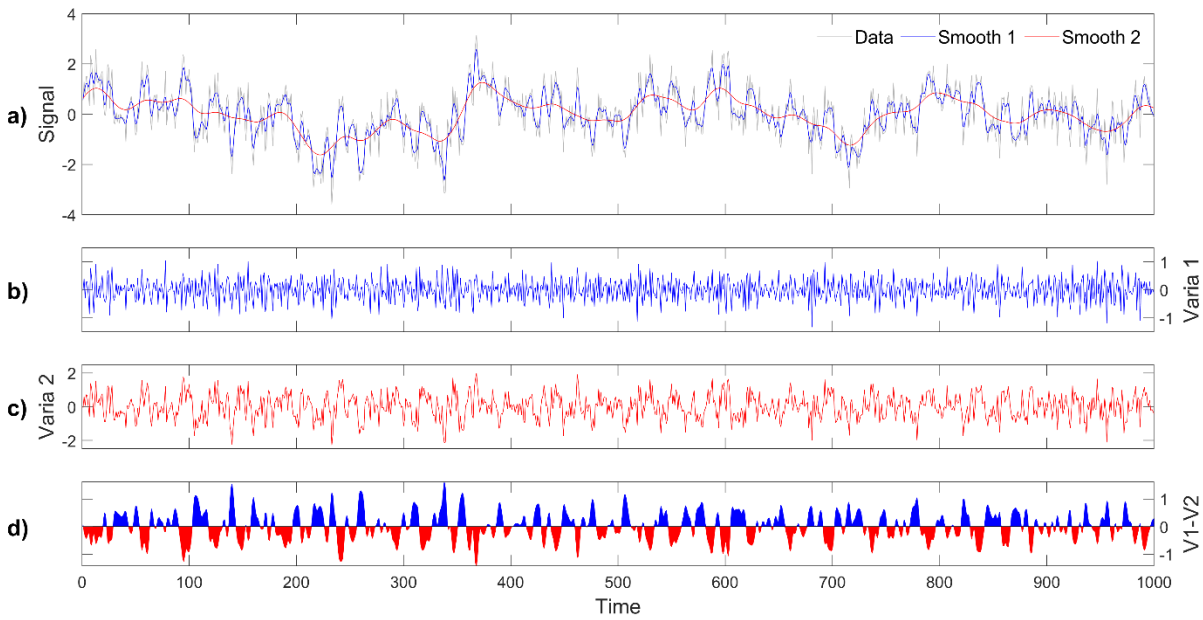

Figure 3. The approximate entropy of simulated time series in the blue ($1/f^{-2}$) to red ($1/f^{2}$) spectrum. See text for further details.

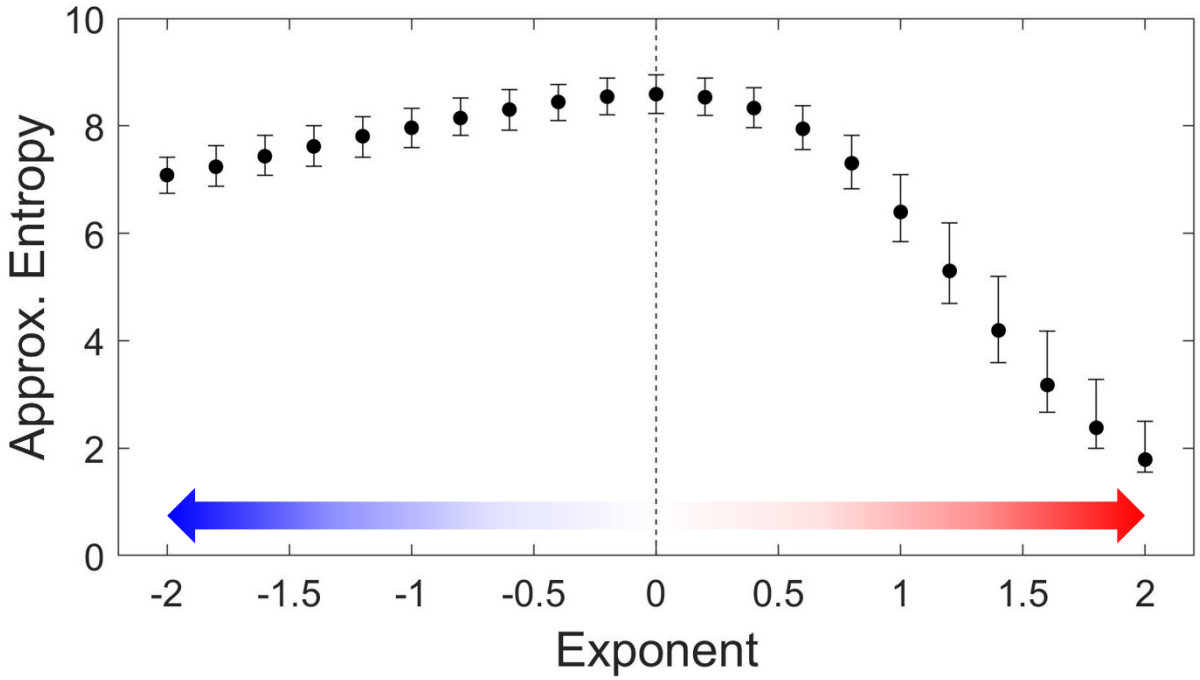

Figure 4. Example result of Simulation 1. (A) shows the original simulated signal. (B) and (D) compare the original change and variability components respectively to those reconstructed via the CVD algorithm; original components are shown in blue, with reconstructed components in red. (C) and (E) show scatterplots of the original and reconstructed change and variability components with Pearson product-moment correlation coefficients between originals and reconstructions; dashed blue lines show isometric relationships.

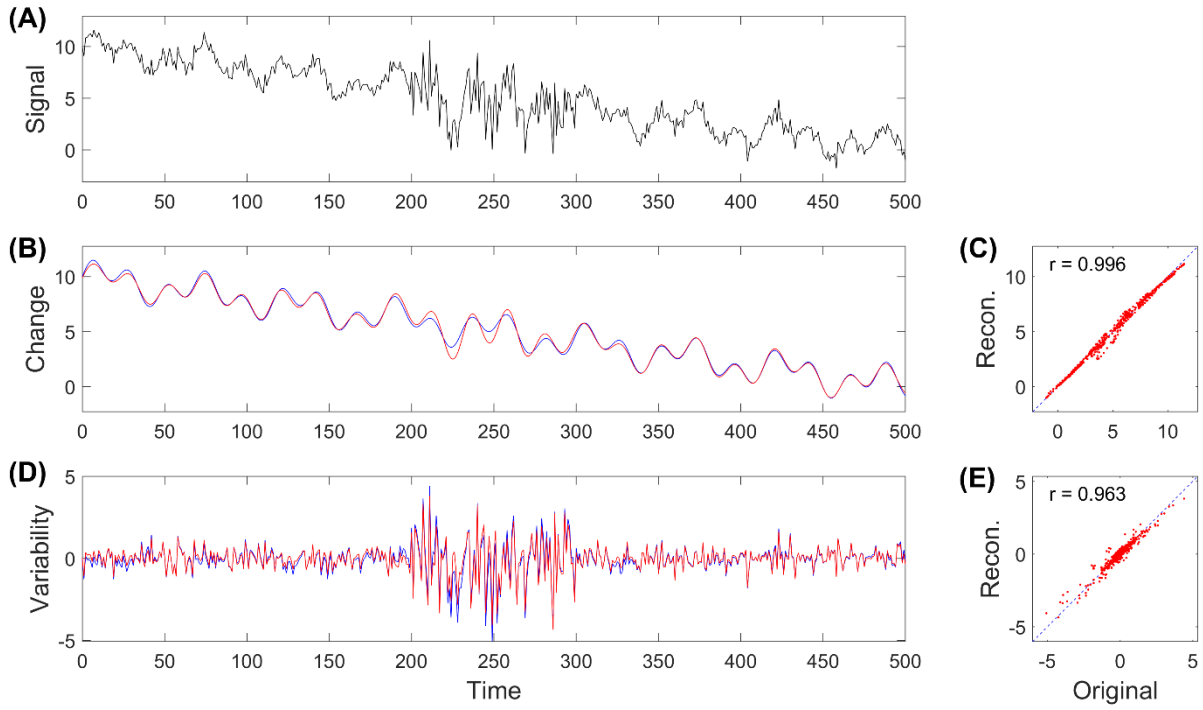

Figure 5. Example result of Simulation 2. (A) shows the original simulated signal. (B) and (D) compare the original change and variability components respectively to those reconstructed via the CVD algorithm; original components are shown in blue, with reconstructed components in red. (C) and (E) show scatterplots of the original and reconstructed change and variability components with Pearson product-moment correlation coefficients between originals and reconstructions; dashed blue lines show isometric relationships.

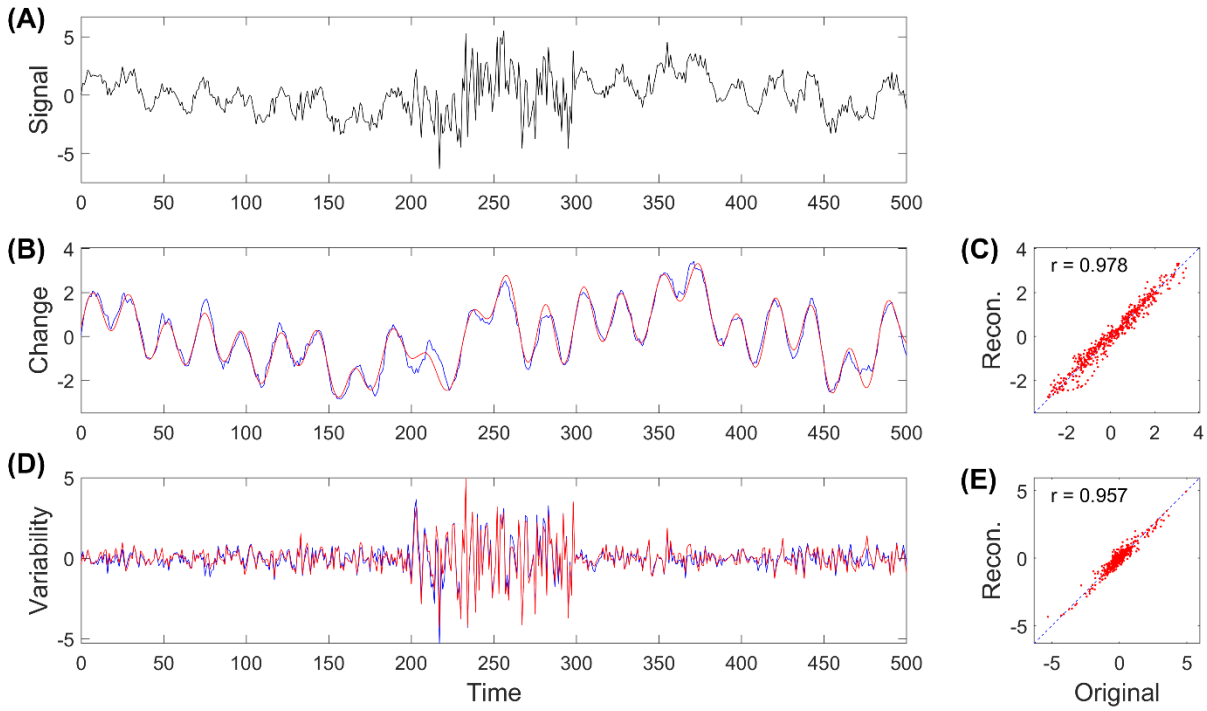

Figure 6. Results of Simulation 3. a), b), and c) show correlation coefficients between original and reconstructed change components of the simulated signals under increasing variance of white noise, red noise, and the sine wave signal respectively. d), e), and f) show equivalent plots for the variability component. Dots indicate medians; whiskers show median absolute deviations.

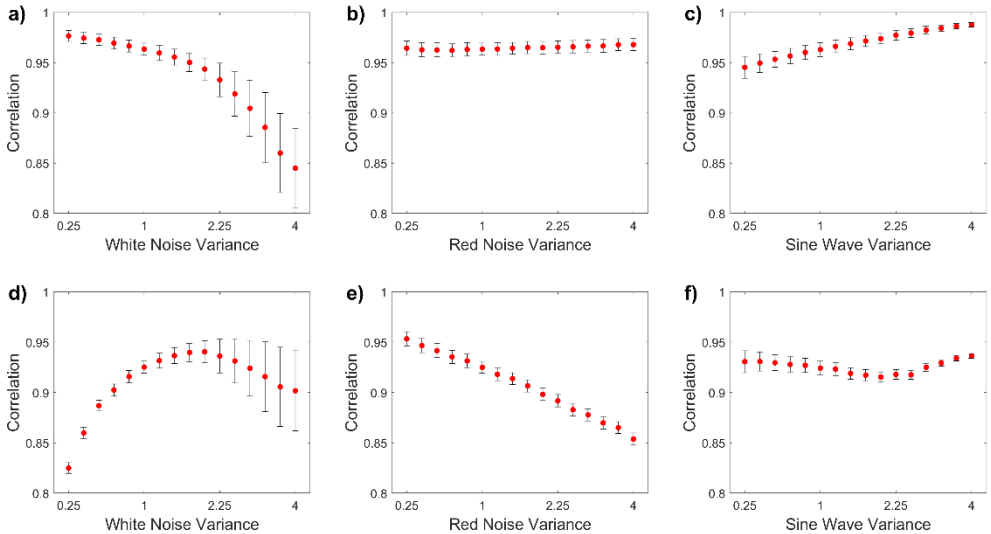

Figure 7. Results of Simulation 4. a) shows variation in ω^* (the number of reconstructed components comprising the 'change') under varying M (embedding dimension). Red lines at notches show medians, boxes show inter-quartile ranges, and whiskers encompass all data. b) plots the average variance-covariance matrix of change signals constructed under varying M (below the anti-diagonal) and variability signals constructed under varying M (above the anti-diagonal).

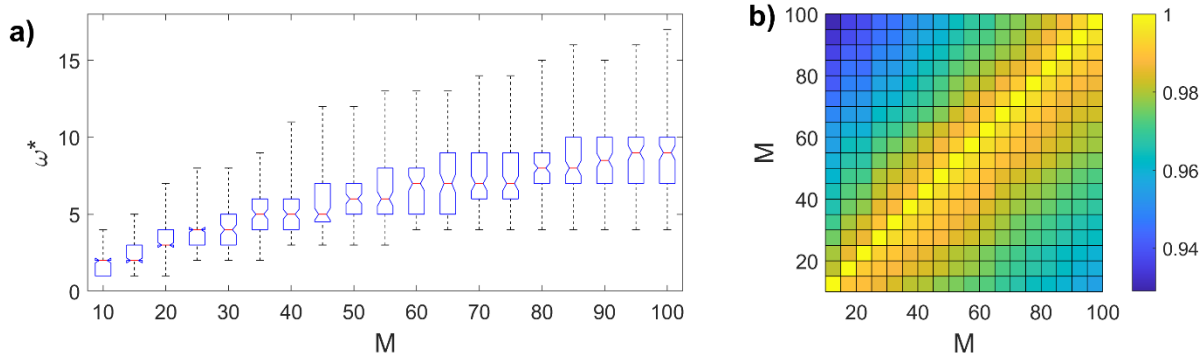

Figure 8. A single example of Simulation 4 output. a) shows the original signal. b) and c) show the 19 estimates of change and variability produced under values of M from 10 to 100 in increments of 5. Note minimal disparities over an order of magnitude difference in M.

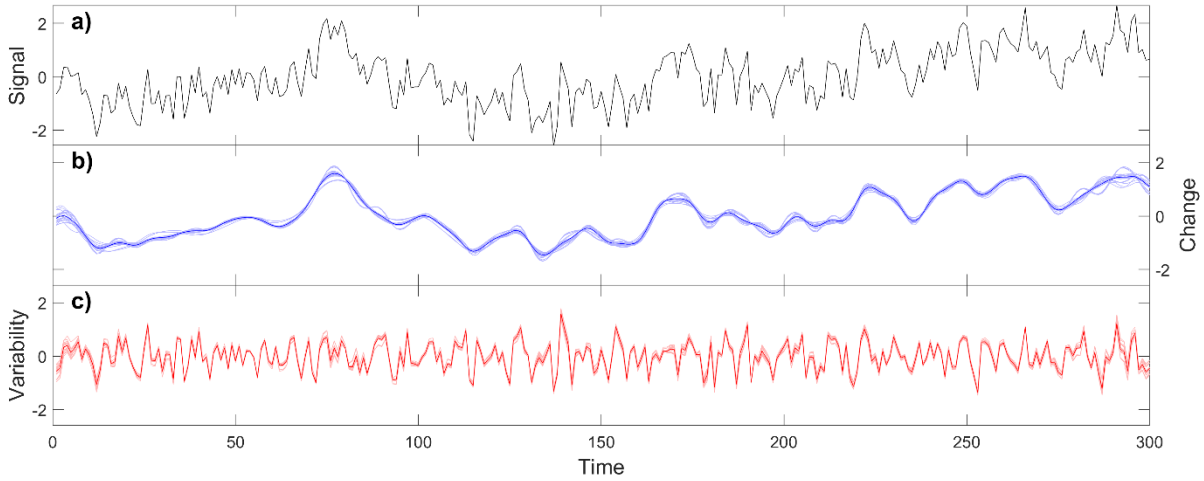

Figure 9. Power spectrum (periodogram) of the change and variability components of the monthly Southern Oscillation Index from 1870 to 2019.

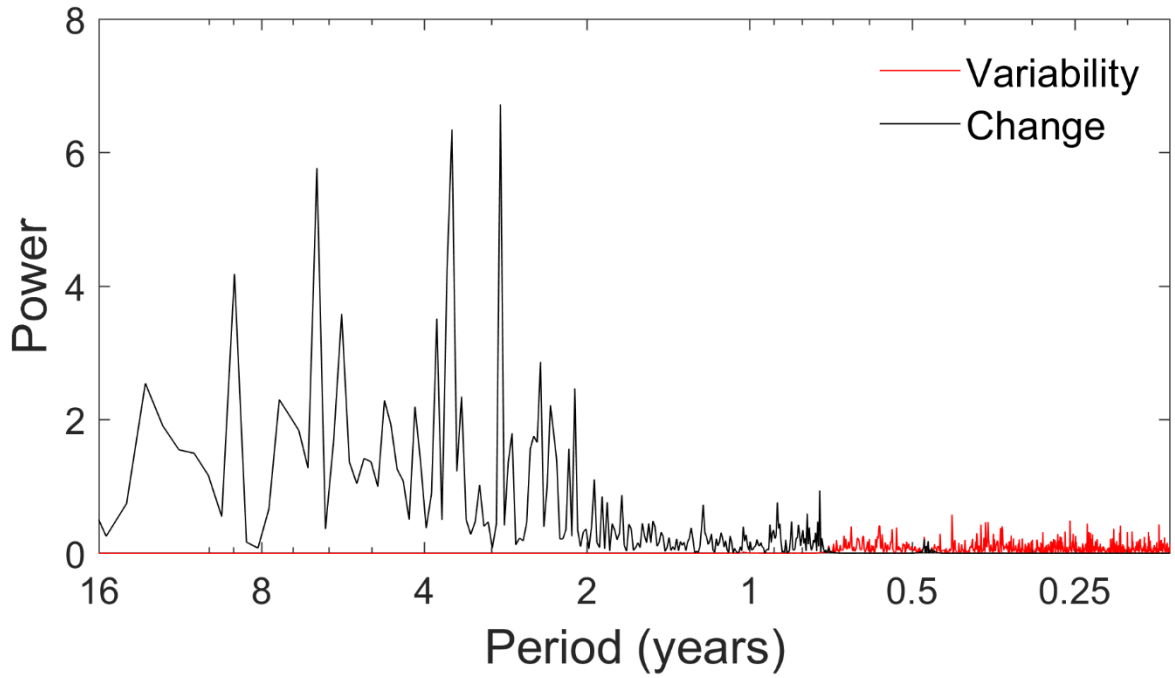

Figure 10. a) the raw monthly SOI from 1870 to 2019 and b) the change component of the SOI over the same period. Orange and yellow squares show 'strong' and 'weak' El Niño months respectively (after Smith and Sardeshmukh 2000). Red and black triangles show true positive and false positive identifications of El Niño months respectively (as per the method of Kiladis and van Loon 1988).

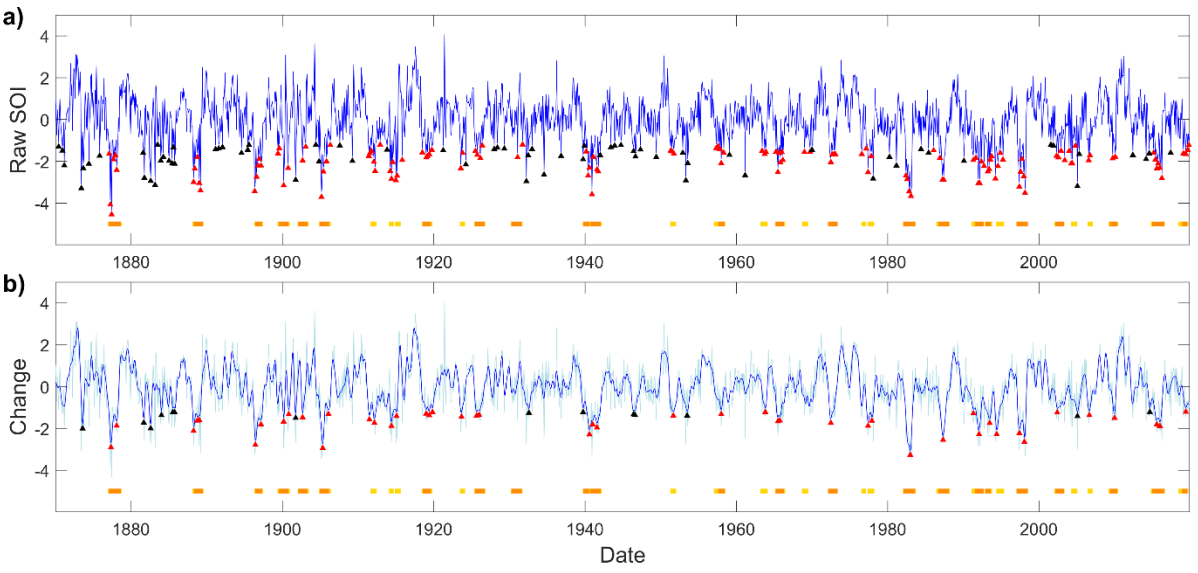

Figure 11. Histograms of inter-event periods for the monthly raw SOI and change component of the SOI over the period 1870-2019.

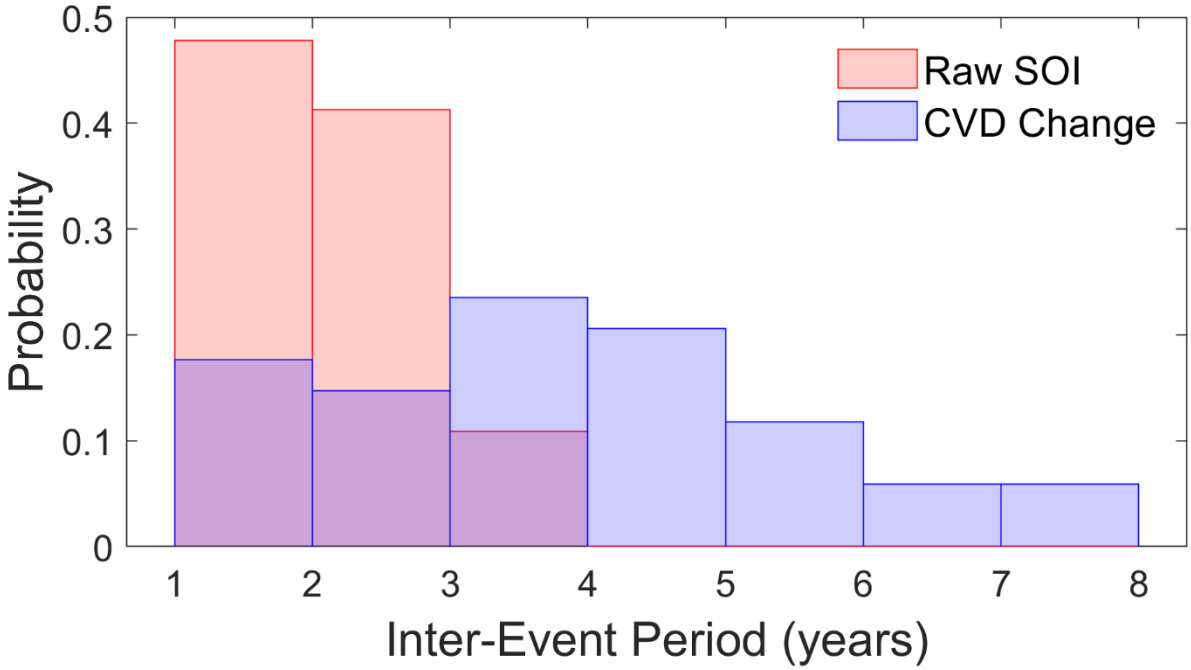

Figure 12. Timelines of major palaeoclimatic and archaeological phases in southwest Asia over the period from 17 ka to 9 ka (b2k) shown with the relevant section of the NGRIP $\delta^{18}O$ record (Rasmussen et al. 2014).

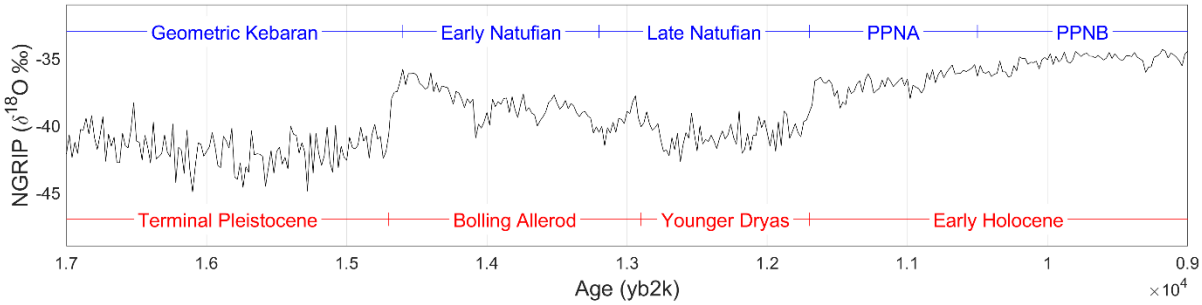

Figure 13. Application of the running Mann-Whitney statistic advocated by Trauth and colleagues (2009) to the absolute first derivative of the variability component. The top panel shows the change component, the middle panel the absolute first derivative of the variability component, and the bottom panel the p-values (as $-\log(p)$) generated via the running Mann-Whitney statistic. Red, green, and blue horizontal bars in the bottom panel show significant transitions at window widths of 50, 100, and 150 data points respectively. The horizontal grey line is at $-\log(0.01)$. Vertical dashed lines show transitions identified as significant under all three window widths simultaneously.

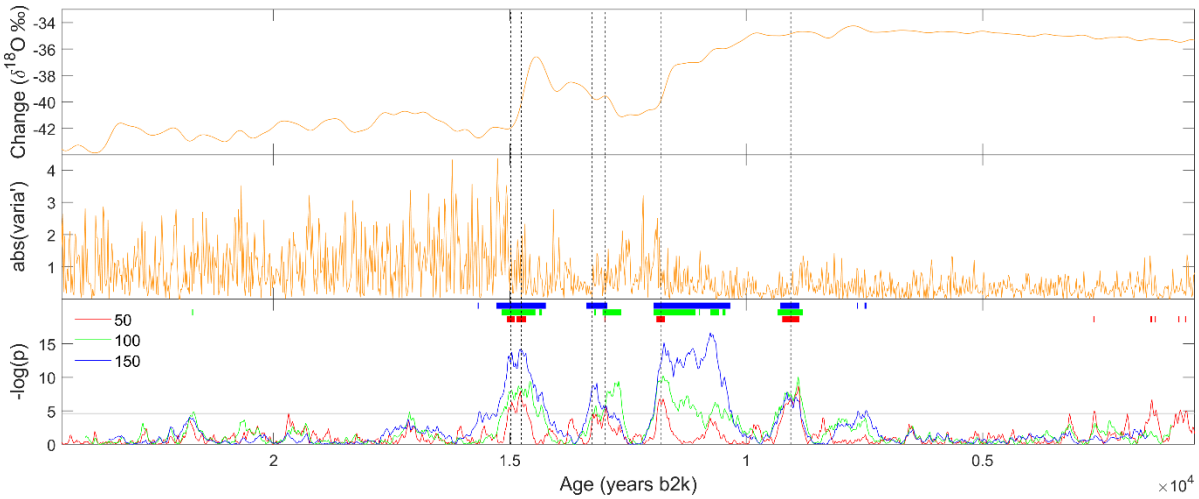

Figure 14. The identified variability transitions aligned with major palaeoclimatic and archaeological phases in southwest Asia and the domestication chronology given by Larson and colleagues (2014). Coloured bars indicate exploitation prior to domestication (grey), management or pre-domestication cultivation (blue) and appearance of morphological changes associated with domestication (red). The kernel density plot summarises the dates of management or pre-domestication cultivation (blue line) and morphological changes associated with domestication (red line). Green arrows indicate decreases in variability; purple arrows indicate increases in variability.

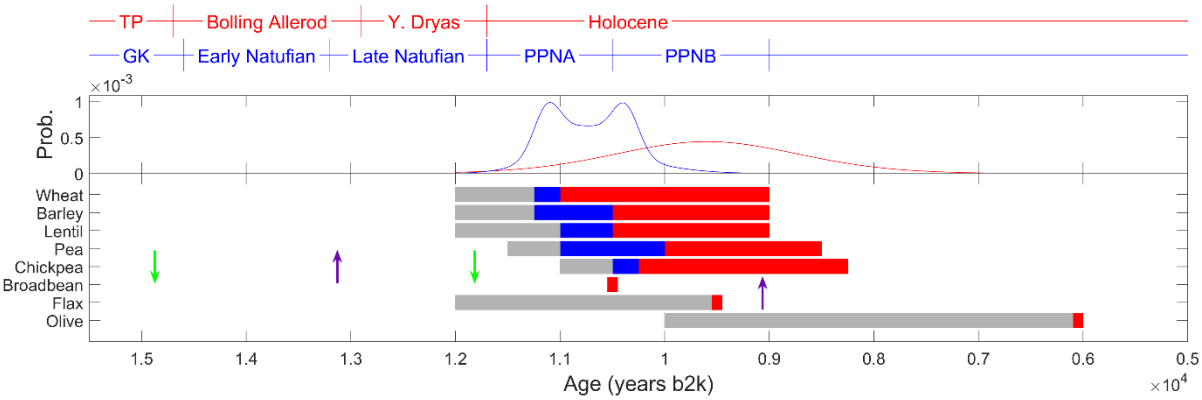

Figure 15. Sigmoid plot fitted to the data on percentages of founder crops found among non-woody plant macro-remains at southwest Asian archaeological sites collated by Arranz-Otaegui and colleagues (2018a). The purple line shows the sigmoid, with the purple region showing the 95% confidence region. Vertical dashed lines show the mean (black) and 95% confidence intervals (grey) of the d parameter dating the significant increase in founder crop percentages. Green arrows indicate decreases in variability; purple arrows indicate increases in variability.

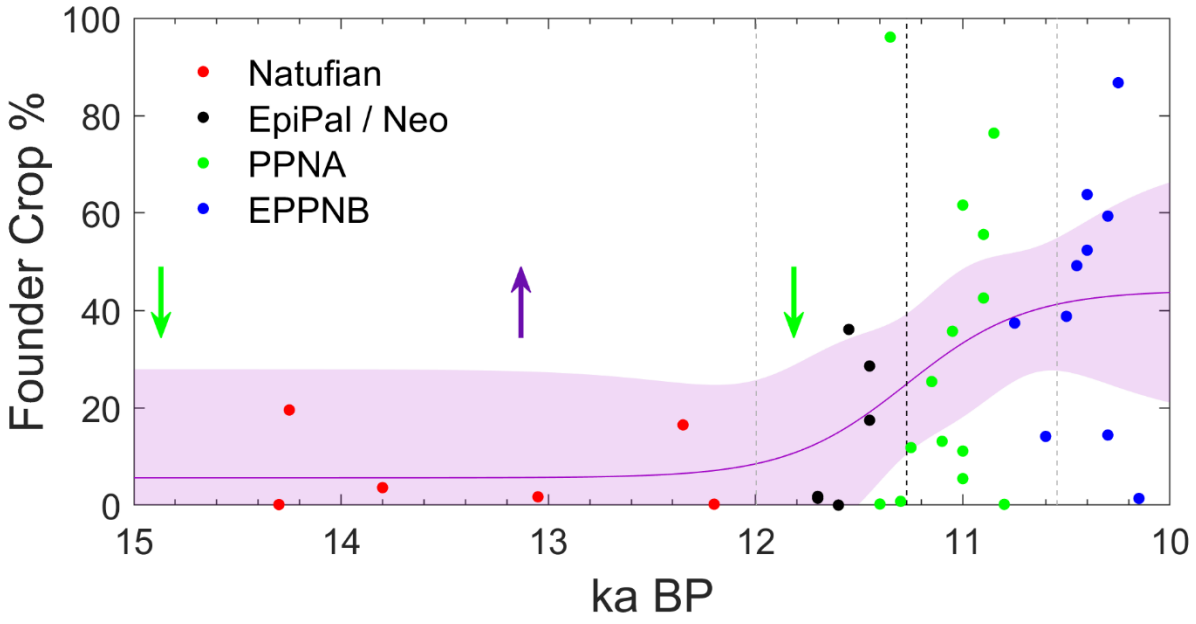

Tables

Table 1. Percentages of false positives using the raw monthly SOI and the change component of the SOI. Results are shown for the entire period from 1870 to 2019, and for the reduced period from 1900 to 2019 (for which records are more reliable).

	Period	Total Months	True Months	False Months	False Pos %
Raw SOI	All	204	134	70	34.31
	From 1900	162	116	46	28.40
Change	All	61	47	14	22.95
	From 1900	48	40	8	16.67

CVD Algorithm

```
% CVD (Change Variability Decomposition) Algorithm
% matt.grove@liverpool.ac.uk
% CVD.m

function [RCSig,Change,Varia] = CVD(t,data,M)
    X = [ones(size(t)) t];
    b = X\data;
    Ltrend = b(1)+b(2)*t;
    data = data-Ltrend;
    Mdata = mean(data);
    data = data-Mdata;
    SDdata = std(data);
    data = data/SDdata;
    N = length(data);
    Y = zeros(N-M+1,M); % Trajectory matrix
    for m = 1:M
        Y(:,m) = data(m:N-M+m); % Embedding
    end
    C = Y'*Y/(N-M+1); % Covariance matrix
    [RHO,LAMBDA] = eig(C); % Eigendecomposition
    LAMBDA = diag(LAMBDA);
    [~,ind] = sort(LAMBDA,'descend');
    RHO = RHO(:,ind);
    PC = Y*RHO; % Principal components
    RC = zeros(N,M); % Reconstructed components
    for m = 1:M
        buf = PC(:,m)*RHO(:,m)';
        buf = buf(end:-1:1,:);
        for n = 1:N % anti-diagonal averaging
            RC(n,m) = mean(diag(buf,-(N-M+1)+n));
        end
    end
    nfft = 2^nextpow2(N);
    Fs = 1/(t(2)-t(1)); % Sampling frequency from t
    wn95 = 0.5*chi2inv(0.95,2);
    d = -1;
    RCSig = -1;
    while d <= 0
        RCSig = RCSig + 1;
        Rec = sum(RC(:,1+RCSig:M),2);
        ftRec = fft(Rec,nfft);
        ftRec = ((abs(ftRec(1:nfft/2,1)).^2)/Fs/N);
        ftRec = [ftRec(1); 2*ftRec(2:end)];
        ftRec = ftRec/(2*(1/Fs));
        mx = max(ftRec);
        d = wn95-mx;
    end
    Change = sum(RC(:,1:RCSig),2)*SDdata+Mdata+Ltrend;
    Varia = sum(RC(:,RCSig+1:end),2)*SDdata;
end
```

Validation Simulation 1

```
% CVD Validation Simulation 1
% CVDValSim1.m
% matt.grove@liverpool.ac.uk
% NOTE: Calls function CVD.m
% NOTE: Simulation is stochastic; each run will produce a different white
% noise signal
% This simulation produces Figure 4 in the paper

clear, clc, close all
t = (0:1:500)';
p1 = 23; p2 = 59;
pr = 1;
```

```
noise = 0.5*randn(length(t),1);
noise(201:300,1) = 4*noise(201:300,1);
signal = -0.02*t+10+sin(2*pi*t/p1)+pr*sin(2*pi*t/p2);
data = signal+noise;
M = 60;
[RCSig,Change,Varia] = CVD(t,data,M);
sws = -0.02*t+10+sin(2*pi*t/23)+sin(2*pi*t/59);
rC = corrcoef(signal,Change);
rC = round(rC(2,1),3);
rV = corrcoef(noise,Varia);
rV = round(rV(2,1),3);

subplot(3,3,[1 2])
mns = min(data);
mxs = max(data);
mn = mns-((mxs-mns)*0.1);
mx = mxs+((mxs-mns)*0.1);
plot(t,data,'k-')
ylim([mn mx])
set(gca,'FontSize',14)
ylabel('Signal','FontSize',18)
text(-45,mx,'(A)','FontSize',20,'FontWeight','bold')

subplot(3,3,[4 5])
mns = min(min(signal),min(Change));
mxs = max(max(signal),max(Change));
mn = mns-((mxs-mns)*0.1);
mx = mxs+((mxs-mns)*0.1);
plot(t,signal,'b-'), hold on
plot(t,Change,'r-'), hold off
ylim([mn mx])
set(gca,'FontSize',14)
ylabel('Change','FontSize',18)
text(-45,mx,'(B)','FontSize',20,'FontWeight','bold')

subplot(3,3,6)
plot([mn mx],[mn mx],'b--'), hold on
scatter(signal,Change,21,'r','Marker','.'), hold off
axis square
xlim([mn mx])
ylim([mn mx])
P = 0.1*abs(mn-mx);
text(mn+P,mx-P,['r = ',num2str(rC)],'FontSize',14)
set(gca,'FontSize',14)
ylabel('Recon.','FontSize',18)
text(mn-((mx-mn)*(180/500)),mx,'(C)','FontSize',20,'FontWeight','bold')

subplot(3,3,[7 8])
mns = min(min(noise),min(Varia));
mxs = max(max(noise),max(Varia));
mn = mns-((mxs-mns)*0.1);
mx = mxs+((mxs-mns)*0.1);
plot(t,noise,'b-'), hold on
plot(t,Varia,'r-'), hold off
set(gca,'FontSize',14)
xlabel('Time','FontSize',18)
ylabel('Variability','FontSize',18)
text(-45,mx,'(D)','FontSize',20,'FontWeight','bold')

subplot(3,3,9)
plot([mn mx],[mn mx],'b--'), hold on
scatter(noise,Varia,21,'r','Marker','.'), hold off
axis square
xlim([mn mx])
ylim([mn mx])
P = 0.1*abs(mn-mx);
text(mn+P,mx-P,['r = ',num2str(rV)],'FontSize',14)
set(gca,'FontSize',14)
```

```
xlabel('Original','FontSize',18)
ylabel('Recon.','FontSize',18)
text(mn-((mx-mn)*(180/500)),mx,'(E)','FontSize',20,'FontWeight','bold')
set(gcf,'color','w')
```

Validation Simulation 2

```
% CVD Validation Simulation 2
% CVDValSim2.m
% matt.grove@liverpool.ac.uk
% NOTE: Calls function CVD.m
% NOTE: Simulation is stochastic; each run will produce different red and
% white noise signals
% This simulation produces Figure 5 in the paper

clear, clc, close all
t = (0:1:500)';
p1 = 23; p2 = 59;
pr = 1;
noise = 0.5*randn(length(t),1);
noise(201:300,1) = 4*noise(201:300,1);
noise = zscore(noise);
t2 = (1:1:256)';
sf = 1;
f = (t2/(2*sf))/length(t2);
len = length(t2);
i = sqrt(-1);
PSD = f.^-2;
amp = sqrt(2*(PSD));
amp(len+1:2*len) = flipud(amp);
r3 = (2*pi)*rand(length(amp),1);
out = amp.*exp(i*r3);
R = real(ifft(out));
R = zscore(R(1:501));
signal = sin(2*pi*t/p1)+pr*sin(2*pi*t/p2)+R;
data = signal+noise;
clearvars -except data signal noise t
M = 60;
[RCSig,Change,Varia] = CVD(t,data,M);

rC = corrcoef(signal,Change);
rC = round(rC(2,1),3);
rV = corrcoef(noise,Varia);
rV = round(rV(2,1),3);

subplot(3,3,[1 2])
mns = min(data);
mxs = max(data);
mn = mns-((mxs-mns)*0.1);
mx = mxs+((mxs-mns)*0.1);
plot(t,data,'k-')
ylim([mn mx])
set(gca,'FontSize',14)
ylabel('Signal','FontSize',18)
text(-45,mx,'(A)','FontSize',20,'FontWeight','bold')

subplot(3,3,[4 5])
mns = min(min(signal),min(Change));
mxs = max(max(signal),max(Change));
mn = mns-((mxs-mns)*0.1);
mx = mxs+((mxs-mns)*0.1);
plot(t,signal,'b-'), hold on
plot(t,Change,'r-'), hold off
ylim([mn mx])
set(gca,'FontSize',14)
ylabel('Change','FontSize',18)
text(-45,mx,'(B)','FontSize',20,'FontWeight','bold')
```

```
subplot(3,3,6)
plot([mn mx],[mn mx],'b--'), hold on
scatter(signal,Change,21,'r','Marker','.'), hold off
axis square
xlim([mn mx])
ylim([mn mx])
P = 0.1*abs(mn-mx);
text(mn+P,mx-P,['r = ',num2str(rC)],'FontSize',14)
set(gca,'FontSize',14)
ylabel('Recon.','FontSize',18)
text(mn-((mx-mn)*(180/500)),mx,'(C)','FontSize',20,'FontWeight','bold')

subplot(3,3,[7 8])
mns = min(min(noise),min(Varia));
mxs = max(max(noise),max(Varia));
mn = mns-((mxs-mns)*0.1);
mx = mxs+((mxs-mns)*0.1);
plot(t,noise,'b-'), hold on
plot(t,Varia,'r-'), hold off
set(gca,'FontSize',14)
xlabel('Time','FontSize',18)
ylabel('Variability','FontSize',18)
text(-45,mx,'(D)','FontSize',20,'FontWeight','bold')

subplot(3,3,9)
plot([mn mx],[mn mx],'b--'), hold on
scatter(noise,Varia,21,'r','Marker','.'), hold off
axis square
xlim([mn mx])
ylim([mn mx])
P = 0.1*abs(mn-mx);
text(mn+P,mx-P,['r = ',num2str(rV)],'FontSize',14)
set(gca,'FontSize',14)
xlabel('Original','FontSize',18)
ylabel('Recon.','FontSize',18)
text(mn-((mx-mn)*(180/500)),mx,'(E)','FontSize',20,'FontWeight','bold')
set(gcf,'color','w')
```

Validation Simulation 3

```
% CVD Validation Simulation 3
% CVDValSim3.m
% matt.grove@liverpool.ac.uk
% NOTE: Calls function CVD.m
% This simulation produces Figure 6 in the paper

clear, clc, close all
tic
t = (0:1:500)';
t2 = (1:1:256)';
sf = 1;
f = (t2/(2*sf))/length(t2);
len = length(t2);
PSD = f.^-2;
amp = sqrt(2*(PSD));
amp(len+1:2*len) = flipud(amp);
sw = zscore(sin(2*pi*t/23)+sin(2*pi*t/59));
vs = 0.5:0.1:2;
iter = 1000;
M = 60;

[ONEC,ONEV] = deal(zeros(iter,length(vs)));
for n = 1:length(vs)
    v = vs(n);
    for m = 1:iter
        noise = randn(length(t),1);
```

```
        noise = v*zscore(noise);
        rpa = (2*pi)*rand(length(amp),1);
        out = amp.*exp(sqrt(-1)*rpa);
        R = real(ifft(out));
        R = zscore(R(1:501));
        CC = sw+R;
        data = CC+noise;
        [~,change,varia] = CVD(t,data,M);
        rC = corrcoef(change,CC);
        rV = corrcoef(varia,noise);
        ONEC(m,n) = rC(1,2);
        ONEV(m,n) = rV(1,2);
    end
end

[TWOC,TWOV] = deal(zeros(iter,length(vs)));
for n = 1:length(vs)
    v = vs(n);
    for m = 1:iter
        noise = randn(length(t),1);
        noise = zscore(noise);
        rpa = (2*pi)*rand(length(amp),1);
        out = amp.*exp(sqrt(-1)*rpa);
        R = real(ifft(out));
        R = v*zscore(R(1:501));
        CC = sw+R;
        data = CC+noise;
        [~,change,varia] = CVD(t,data,M);
        rC = corrcoef(change,CC);
        rV = corrcoef(varia,noise);
        TWOC(m,n) = rC(1,2);
        TWOV(m,n) = rV(1,2);
    end
end

[THREEC,THREEV] = deal(zeros(iter,length(vs)));
for n = 1:length(vs)
    s = sw*vs(n);
    for m = 1:iter
        noise = randn(length(t),1);
        noise = zscore(noise);
        rpa = (2*pi)*rand(length(amp),1);
        out = amp.*exp(sqrt(-1)*rpa);
        R = real(ifft(out));
        R = zscore(R(1:501));
        CC = s+R;
        data = CC+noise;
        [~,change,varia] = CVD(t,data,M);
        rC = corrcoef(change,CC);
        rV = corrcoef(varia,noise);
        THREEC(m,n) = rC(1,2);
        THREEV(m,n) = rV(1,2);
    end
end
tt = toc;
save ValSim3.mat vs ONEC ONEV TWOC TWOV THREEC THREEV tt

%% Plot

clear, clc, close all
load ValSim3.mat
xt = 0.5:0.5:2;
medONEC = median(ONEC);
madONEC = mad(ONEC,1);
medONEV = median(ONEV);
madONEV = mad(ONEC,1);
medTWOC = median(TWOC);
madTWOC = mad(TWOC,1);
```

```
medTWOV = median(TWOV);
madTWOV = mad(TWOC,1);
medTHREEC = median(THREEC);
madTHREEC = mad(THREEC,1);
medTHREEV = median(THREEV);
madTHREEV = mad(THREEC,1);

subplot(2,3,1)
errorbar(vs,medONEC,madONEC,'o','Color','k','MarkerSize',5,...
    'MarkerEdgeColor','red','MarkerFaceColor','red')
xlim([0.4 2.1])
xticks(xt)
xticklabels({'0.25','1','2.25','4'})
ylim([.8 1])
set(gca,'FontSize',12)
xlabel('White Noise Variance','FontSize',16)
ylabel('Correlation','FontSize',16)
text(.1,1,'a)','FontSize',20,'FontWeight','bold')

subplot(2,3,2)
errorbar(vs,medTWOC,madTWOC,'o','Color','k','MarkerSize',5,...
    'MarkerEdgeColor','red','MarkerFaceColor','red')
xlim([0.4 2.1])
xticks(xt)
xticklabels({'0.25','1','2.25','4'})
ylim([.8 1])
set(gca,'FontSize',12)
xlabel('Red Noise Variance','FontSize',16)
ylabel('Correlation','FontSize',16)
text(.1,1,'b)','FontSize',20,'FontWeight','bold')

subplot(2,3,3)
errorbar(vs,medTHREEC,madTHREEC,'o','Color','k','MarkerSize',5,...
    'MarkerEdgeColor','red','MarkerFaceColor','red')
xlim([0.4 2.1])
xticks(xt)
xticklabels({'0.25','1','2.25','4'})
ylim([.8 1])
set(gca,'FontSize',12)
xlabel('Sine Wave Variance','FontSize',16)
ylabel('Correlation','FontSize',16)
text(.1,1,'c)','FontSize',20,'FontWeight','bold')

subplot(2,3,4)
errorbar(vs,medONEV,madONEV,'o','Color','k','MarkerSize',5,...
    'MarkerEdgeColor','red','MarkerFaceColor','red')
xlim([0.4 2.1])
xticks(xt)
xticklabels({'0.25','1','2.25','4'})
ylim([.8 1])
set(gca,'FontSize',12)
xlabel('White Noise Variance','FontSize',16)
ylabel('Correlation','FontSize',16)
text(.1,1,'d)','FontSize',20,'FontWeight','bold')

subplot(2,3,5)
errorbar(vs,medTWOV,madTWOV,'o','Color','k','MarkerSize',5,...
    'MarkerEdgeColor','red','MarkerFaceColor','red')
xlim([0.4 2.1])
xticks(xt)
xticklabels({'0.25','1','2.25','4'})
ylim([.8 1])
set(gca,'FontSize',12)
xlabel('Red Noise Variance','FontSize',16)
ylabel('Correlation','FontSize',16)
text(.1,1,'e)','FontSize',20,'FontWeight','bold')

subplot(2,3,6)
```

```
errorbar(vs,medTHREEV,madTHREEV,'o','Color','k','MarkerSize',5,...
    'MarkerEdgeColor','red','MarkerFaceColor','red')
xlim([0.4 2.1])
xticks(xt)
xticklabels({'0.25','1','2.25','4'})
ylim([.8 1])
set(gca,'FontSize',12)
xlabel('Sine Wave Variance','FontSize',16)
ylabel('Correlation','FontSize',16)
text(.1,1,'f)','FontSize',20,'FontWeight','bold')
set(gcf,'color','w')
```

Validation Simulation 4

```
% CVD Validation Simulation 4
% CVDValSim4.m
% matt.grove@liverpool.ac.uk
% NOTE: Calls function CVD.m
% This simulation produces Figures 7 and 8 in the paper

clear, clc, close all
m = 256;
t = (1:1:m)';
sf = 1;
f = (t/(2*sf))/length(t);
len = length(t);
i = sqrt(-1);
PSD = f.^-1;
amp = sqrt(0.5*abs(PSD));
amp(len+1:2*len) = flipud(amp);
T = (1:1:300)';
MS = 10:5:100;
iter = 100;
[VS,CS,sVS,sCS] = deal(zeros(length(T),length(MS)));
RS = zeros(length(iter),length(MS));
sENV = zeros(length(T),1);
[AllVs,AllCs] = deal(zeros(length(MS),length(MS),length(iter)));
for m = 1:iter
    r3 = (2*pi)*rand(length(amp),1);
    out = amp.*exp(i*r3);
    K = real(ifft(out));
    K = zscore(K(1:300));
    for n = 1:length(MS)
        M = MS(n);
        [RS(m,n),CS(:,n),VS(:,n)] = CVD(T,K,M);
    end
    if m == 1
        sVS = VS;
        sCS = CS;
        sENV = K;
    end
    AllVs(:,:,m) = corrcoef(VS);
    AllCs(:,:,m) = corrcoef(CS);
end
V = mean(AllVs,3);
C = mean(AllCs,3);
R = mean(RS);
Rlow = prctile(RS,25);
Rhi = prctile(RS,75);
save VaryingM.mat MS C V sVS sCS R T K sENV Rlow Rhi RS

%% Figure 7

clear, clc, close all
load VaryingM.mat
a = triu(C);
b = tril(V);
```

```
z = max(a,b);
neg = R-Rlow;
pos = Rhi-R;

subplot(2,2,1)
boxplot(RS,MS,'Notch','on','Whisker',inf)
set(gca,'xtick',1:2:19,'xticklabel',{'10','20','30','40','50','60','70','80','90','
100'})
set(gca,'FontSize',14)
xlabel('M','FontSize',18)
ylabel('\omega*','FontSize',18)
ylim([0 18])
text(-2,17,'a)','FontSize',20,'FontWeight','bold')

subplot(2,2,2)
pcolor(MS,MS,z)
axis square
colorbar
set(gca,'FontSize',14)
xlabel('M','FontSize',18)
ylabel('M','FontSize',18)
text(-15,100,'b)','FontSize',20,'FontWeight','bold')
set(gcf,'color','w')

%% Figure 8

clear, clc, close all
load VaryingM.mat
MeanC = mean(sCS,2);
MeanV = mean(sVS,2);

subplot(3,1,1)
plot(T,sENV,'k-')
set(gca,'FontSize',14)
xticklabels({})
ylabel('Signal','FontSize',18)
yl = ylim;
text(5,0.8*yl(2),'a)','FontSize',20,'FontWeight','bold')

subplot(3,1,2)
plot(T,sCS,'Color',[.7 .7 1]), hold on
plot(T,MeanC,'b-'), hold off
set(gca,'FontSize',14)
xticklabels({})
ax = gca;
ax.YAxisLocation = 'right';
ylabel('Change','FontSize',18)
ylim(yl)
text(5,0.8*yl(2),'b)','FontSize',20,'FontWeight','bold')

subplot(3,1,3)
plot(T,sVS,'Color',[1 .7 .7]), hold on
plot(T,MeanV,'r-'), hold off
set(gca,'FontSize',14)
ylabel('Variability','FontSize',18)
xlabel('Time','FontSize',18)
ylim(yl)
text(5,0.8*yl(2),'c)','FontSize',20,'FontWeight','bold')
set(gcf,'color','w')
```